SYNOPTIC DRIVERS OF STORM SURGE IN KOTZEBUE SOUND

By

Austin E. Cross

RECOMMENDED:

_____

_____

_____

Advisory Committee Chair

_____

Chair, Department of Atmospheric Sciences

APPROVED:

_____

Dean, College of Natural Science and Mathematics

_____

Dean of the Graduate School

_____

Date

SYNOPTIC DRIVERS OF STORM SURGE IN KOTZEBUE SOUND

A

THESIS

Presented to the Faculty

of the University of Alaska Fairbanks

in Partial Fulfillment of the Requirements

for the Degree of

MASTER OF SCIENCE

By

Austin E. Cross, B.S.

Fairbanks, Alaska

August 2010

Abstract

Coastal flooding due to storm surge is a serious danger for communities and industry in western Alaska. The purpose of this study is to gain an understanding of which storm tracks lead to the greatest surge, whether certain areas are more vulnerable than others due to local scale features, and what currents are associated with surge events. Kotzebue Sound was chosen as the area of focus on the basis of physical and social factors. Physically, its bathymetry, topography, and coastal orientation make it particularly susceptible to surge. Socially, this region possesses a range of affected coastal groups, including heavy industry and subsistence communities. The study was performed using the ADvanced CIRCulation (ADCIRC) coastal circulation and surge model forced with idealized storm scenarios.

Results from the study suggest the utility of applying a surge model to learn about water run up, set down and induced current on the Alaskan coast. Local flooding peculiarities were found in Hotham Inlet, which could have potential impacts on a sensitive ecosystem. Noticeable differences were found in surge magnitude and distribution between storms of different ground track speed, as well as small changes in track location.

Table of Contents

Page

List of Figures

Page

List of Tables

Page

List of Appendices

Page

Acknowledgements

I would like to thank my advisor Dr. David Atkinson for all of his guidance and support. I also thank my committee members, Drs. Kenneth Sassen and Harper Simmons, for their comments and suggestions. Thanks to Dr. Brian Blanton of the Renaissance Computing Institute for his assistance in getting the ADCIRC model to run stably. Thanks to Ryan Woodard for his UAF thesis LaTeX class, which greatly aided in formatting this document. I thank my friends and colleagues at the university and at the National Weather Service forecast office for their encouragement and support. Last, but certainly not least, I thank my parents, Jay and Uta Cross.

This project was funded by National Oceanic and Atmospheric Administration (NOAA) grant NA06OAR4600179 titled "Social Vulnerability to Climate Change in the Alaskan Coastal Zone" and by NOAA's National Weather Service through their Student Career Experience Program.

Chapter 1

Introduction

Coastal flooding is one of the leading causes of property damage in Alaska (Mason et al., 1997). Storm surge, also called storm tide, is a temporary increase in coastal water level caused by meteorological influences, and is measured as the difference between expected tide and actual water level.

Storm surges can impact the coast in several ways. Most significantly, storm surges inundate low-lying areas. As much as 84% of the Alaska population is situated in close proximity to the coast (US Census Bureau, 2009). Many of Alaska's coastal communities are located at or near sea level in flat areas along the coast, putting them in particular danger. Most vulnerable are villages built on sand spits, barrier island and river deltas (Mason et al., 1997), which often are the preferred locations because of the logistical requirements for airport construction. River deltas, such as the expansive Yukon-Kuskokwim delta on the western Alaska coast, are particularly vulnerable – almost any high-water event can quickly inundate large areas because the relief is very low. Wave damage along erosion-prone bluff coastlines is also exacerbated.

Surge events increase the reach of waves in two ways: by raising their effective height above sea level, and by allowing larger waves in depth-limited coastal environments. Waves that ride in at an elevated sea level can break against structures or the bases of bluffs normally above their reach. Infrastructure can be damaged both by direct wave action and the erosion of soil underneath. Much of Alaska's coastline is generally vulnerable to erosion,

but storm surge events put them at particular risk. Surge events can also be problematic for terrestrial ecosystems. For example, the introduction of sea water into coastal areas normally exposed only to fresh water can cause a significant die off of vegetation, as observed in a Beaufort Sea storm that impacted the Mackenzie Delta (Reimnitz and Maurer, 1979). As well, many of the low-relief coastal deltas are important migratory bird sanctuaries (Hupp et al., 2008). Finally, even relatively minor surges can hydrodynamically dam rivers, causing flooding along the river banks due to a backed up river.

The heavy coastal use in western and northern Alaska is made up of more than residences. The coast serves as an important transportation hub because overland transportation is difficult; in fact, western Alaska is not even serviced by a road network. Towns receive most of their resupply via small port facilities. This includes bulk cargo, especially fuel, which is taken to coastal communities by barge in the summer to save on shipping costs. Heavy industry, including the Red Dog Mine operated by Teck Alaska Inc., the largest open pit zinc mine in the world, relies on its Chukchi Sea port to ship its output. Without a road or rail link to the North American heartland, these facilities have no choice but to locate by the ocean, vulnerable to surge.

Preparation for coastal flooding is difficult and expensive, particularly in remote areas. Along coastlines where flooding is the only real concern, the year-to-year threat remains relatively constant. However along erosion-prone coasts, erosion is continually removing material, which exposes to danger areas that were previously set back from the coastline and makes the adoption of some form of remedial action a pressing concern. However it is

also an expensive concern - cost for seawall construction in the contiguous United States has been estimated to range from $150 to $4000 per linear foot (Mendelsohn and Neumann, 2004), and the wall in Nome, Alaska, cost as much as $10,000 per linear foot. Relocation is another option, but it can be even more costly. The US Army Corps of Engineers estimates the cost of relocating the village of Newtok, consisting of 315 residents, at up to $130 million (US Army Corps of Engineers Alaska District, 2006). Many villages are home to residents who have lived in the area for generations making relocation less of an option. Besides the expense, most villages are culturally tied to these locations which can make these options very difficult emotionally.

A longer-term threat to coastal areas around the globe has been emerging during the 20th century as global average sea levels rose between 1 and 2 mm yr^{-1}. Satellite measurements suggest that, between 1993 and 2000, sea levels rose at an even more rapid rate of around 2.5 mm yr^{-1} (Cabanes et al., 2001). The Intergovernmental Panel on Climate Change (IPCC) Fourth Assessment Report concluded that by 2100, global warming will ultimately result in a sea level increase of 19 to 58 cm (Parry, 2007). Given the same storm forcing, higher base line sea level will cause potentially greater damage (Lowe and Gregory, 2005).

Another recent trend that serves to exacerbate potential storm surge and erosion damage is the loss of sea ice due to climate change. The average winter sea ice maximum extends south to the Yukon-Kuskokwim Delta beginning in the fall. In recent years, sea ice area and thickness have been decreasing (Parkinson et al., 1999). Sea ice acts in several ways

to mitigate wave and surge action: it can dampen wave action, keeping seas low and preventing surge, and also reduce the area of sea susceptible to fetch, and shorefast ice armors the coast against wave driven damage. However, thin or unconsolidated ice can pose as much of a hazard as non-existent sea ice, as more powerful storms can break up the ice and create open water conditions. The length of freezeup has been decreasing as well: with the later onset of sea ice cover, more areas of coastline become vulnerable to winter storms for a longer period of time. Atkinson (2005) reported that, over the circumarctic marginal seas, the storms with the greatest windspeed/duration damage-causing potential occur in the Chukchi Sea region in the fall/early winter season. If water is open, or nearly so, these strong late season storms have more potential to cause damaging surge.

Surge combined with sea ice can be very destructive. A cannery and dock were completely destroyed in Naknek, Alaska when a surge floated and drove ashore ice that was bonded to the dock piling (D. E. Atkinson 2009, personal communication).

Wise et al. (1981) found that intense storms can produce 12 ft surge on almost any portion of the western Alaska coast. Most storms do not exceed such heights, however they have on occasion. A November 1974 storm that struck Nome caused significant flood damage, despite the presence of a seawall constructed in 1951. Water levels reached 4.0 m (13.2 ft), with 3.8 m (12.5 ft) attributable to storm surge (Fathauer, 1975), and a storm in October 2004 generated a 10.5 ft surge at Nome (Larsen et al., 2006).

While it is known that surge caused flooding has led to millions in damage, it is thought that many coastal flood events go unreported (Wise et al., 1981). This makes development

of a detailed surge climatology difficult, which means it is also hard to determine which type of storm events are most potentially problematic for a given area.

1.1 Previous work on storm surges in Alaska

Previous work focussing on surge analysis in Alaska, beyond descriptive overviews of selected storms, is limited.

Schafer (1966) developed a finite difference model to analyze an October 1963 storm in Barrow, Alaska that excluded the influence of tides. The grid was 10×15 with a resolution of 76 km ($0.\bar{6}$ degree latitude), and the coastline was treated as two straight lines. They were able to reproduce an approximation of the large scale effects, but conceded that much higher resolution was needed for the gentle slope off Barrow.

A statistical model was developed from the Alaska storm surge climatology developed by Wise et al. (1981). Regression analysis was used to correlate surge height with various parameters. The accuracy of the model results are limited (Blier et al., 1997).

Kowalik (1984) developed a vertically integrated surge model with a resolution of $0.\bar{3}$ degree latitude by 1 degree longitude for the Beaufort and Chukchi Seas. They tested the model on three existing storms and found good agreement with measured sea level from gauges in the Beaufort Sea. Johnson and Kowalik (1986) followed up with a similar model of the Bering Sea and Norton Sound.

More recently, a numerical solution was examined when Blier et al. (1997) tested the National Oceanicic and Atmospheric Administration (NOAA) extratropical surge (E-T surge) model on surge events in Norton Sound, contrasting the results with water levels

observed at Nome. The E-T surge model, which is based on the Sea, Lake, and Overland Surges for Hurricanes (SLOSH) model that is designed for tropical use, did show good agreement with observations for cases of longer duration storm events. The E-T Surge model is used operationally by National Weather Service forecasters for surge guidance, as forced with atmospheric parameters provided by the Global Forecast System (GFS) model. An important limitation of this model is that the forecasts have limited resolution and are unable to resolve flow in smaller waterways. Operationally, it also means that forecast points may not be close to where they are needed (Colle et al., 2008).

1.2 Surge mechanics

Wind driven transport is the most important driver of storm surge. At the interface of the ocean and atmosphere, the more rapidly moving but less viscous air transfers momentum to the slower moving water. This creates a surface stress whereby the water gets dragged along by the wind. This process initiates wave activity but it also entrains the surface mass of water. Surface stress varies with the speed and drag of the water surface, and may be expressed as a vector parallel to the direction of the wind forcing. The area of applied wind stress is referred to as fetch. Longer periods of wind stress and larger areas of fetch allows a greater mass of water to be entrained, which contributes to larger resultant storm surge.

Due to the rotation of the earth, the apparent Coriolis force causes the water to move to the right of the forcing in the northern hemisphere. The resultant surface currents are therefore directed at about a 30 degree angle to the right of the wind (Williams et al., 1973). Each layer of the water acts on the layer below with slightly weaker force due to drag and

the layer below moves to the right of its respective forcing. This effect is known as the Ekman spiral, and results in transport in the deep ocean to be nearly 90 degrees to the right of the wind. In continental shelf areas, the effect is lessened, causing transport closer to 45 degrees right of the wind forcing. In shallow waters, currents throughout the depth tend to approximately parallel the wind due to the strong effect of bottom friction forcing (Pickard and Pond, 1983).

Atmospheric pressure exerts a direct but minor effect, however its inclusion is an important element of atmospheric forcing of the sea state. Determination of final correct water elevations must consider this element. Lower pressure physically draws water levels up in what is called the inverse barometer effect. This effect acts to increase sea level, even when wind driven transport is dampened by sea ice (Wise et al., 1981). In deep water, an elevation change of approximately 1 cm can be expected for each millibar of atmospheric pressure decrease (Anthes, 1982). Given the strength of many storms in the Alaska region – they can drop to 940 hPa – this consideration should not be overlooked.

Bathymetry has a large effect on the potential surge resulting from a given atmospheric forcing. Areas with a narrow shelf or otherwise rapid rise to shore produce little surge as excess water is driven up quickly and can rapidly dissipate. In areas with a large, gently sloping continental shelf, like the Bering and Chukchi Seas, water piles up and is pushed upward like a wedge.

1.3 Motivation

It is the overall objective of this study to delineate case-study atmospheric drivers and link them to their particular, associated surge impacts for a specific area of the western Alaska coast. Several research focus questions guide this effort:

1. What storm track is most problematic and why. This area can be affected by storms moving along several main tracks at different ground speeds and with different wind profiles. Determining the type of storm system able to cause the greatest impact is of particular interest.

2. Are there local flooding peculiarities. At a local scale there are barrier island/lagoon systems. Determining whether water areas behind topography will remain elevated is important, e.g. for salinity and biological mixing considerations.

3. What are the currents associated with surges. Gaining better understanding of the surface currents that arise as water mass is displaced by the winds is also important for erosional and human safety issues.

The focus area is Kotzebue Sound, north of the Bering Strait. This area was selected for several reasons:

1. Its entire offshore vicinity is a shelf zone which makes it highly susceptible to surge, a fact demonstrated repeatedly in the past.

2. It presents a funnel shape which can potentially enhance a surge effect.

3. It has a range of coastal affected groups, including small subsistence villages (e.g. Shishmaref, Deering), a large hub town (Kotzebue), and industrial inhabitants (Teck Alaska Inc.), all of whom are exposed to risk from surge activity.

This work will be accomplished using the ADvanced CIRCulation (ADCIRC) coastal circulation and surge model to test different synoptic situations and examine the resulting surge. Using the model, data may be obtained for any number of sites; thus results will be shared with the NOAA National Weather Service Weather Forecast Office (WFO) that is responsible for this area (the Fairbanks WFO).

Chapter 2

Methodology

2.1 Overview and theory

Simulations in this study are performed with the ADCIRC Coastal Circulation and Storm Surge Model. ADCIRC is short for Advanced Circulation Model for Oceanic, Coastal, and Estuarine Waters. It is a computational fluid dynamics modeling environment that offers two and three dimensional finite element solution domains. Using an unstructured grid with finite elements, resolution is flexible over the domain allowing finer resolution in areas where greater accuracy is required. For this study, the two dimensional depth integrated (2DDI) option was used.

The model solves the generalized wave-continuity equation (GWCE) formulation of the depth integrated continuity equation and uses the two dimensional momentum equations to calculate depth averaged horizontal velocity.

Pre-processing, model setup and grid generation were provided by the Surface Water Modeling System (SMS) version 10 from Aquaveo. Wind and pressure grid inputs were constructed using a custom National Center for Atmospheric Research (NCAR) Command Language (NCL) program. Post-processing and graphics were done with SMS, R and NCL.

Computation is intensive and computing time can be a limiting factor. On a Pentium 4 desktop, a single three day model run at a time step of 5 seconds takes around four hours. ADCIRC allows for the use of parallel computation by use of domain decomposition. The input is decomposed into smaller parts and solved in parallel to allow a great increase in

performance. Taking advantage of this, once the input fields were established, ADCIRC was re-compiled on the 2280-processor Sun Opteron cluster "midnight" platform at the Arctic Region Supercomputing Center. The simulations were then transferred over which greatly reduced run times because multiple nodes could be used.

ADCIRC-2DDI solves the non-conservative momentum equations and the continuity equation in the GWCE. The spherical equations are mapped into recitlenear coordinates using the Carte Parallelogrammatique Projection (CPP).

The non-conservative, vertically integrated momentum equation in the latitudinal direction is:

$$\frac{\partial U}{\partial t}+\frac{1}{R\cos\theta}U\frac{\partial U}{\partial \lambda}+\frac{1}{R}V\frac{\partial U}{\partial \theta}-\left(\frac{tan\theta}{R}U+f\right)V= -\frac{1}{R\cos\theta}\frac{\partial}{\partial \lambda}\left[\frac{p_s}{p_0}+g(\zeta-\alpha\eta)\right]+\frac{1}{H}M_\lambda+\frac{\tau_{s\lambda}}{\rho_0 H}-\tau_* U \tag{2.1}$$

and in the longitudinal direction is:

$$\frac{\partial V}{\partial t}+\frac{1}{R\cos\theta}U\frac{\partial V}{\partial \lambda}+\frac{1}{R}V\frac{\partial U}{\partial \theta}-\left(\frac{tan\theta}{R}U+f\right)U= -\frac{1}{R\cos\theta}\frac{\partial}{\partial \lambda}\left[\frac{p_s}{p_0}+g(\zeta-\alpha\eta)\right]+\frac{1}{H}M_\theta+\frac{\tau_{s\lambda}}{\rho_0 H}-\tau_* V \tag{2.2}$$

where

ϕ, λ are latitude and longitude

U, V are depth averaged horizontal velocity

H is total water column

h is bathymetric depth

ζ is free surface elevation

R is radius of Earth

f is Coriolis parameter

p_s is atmospheric pressure at free surface

p_0 is reference density of water

g is acceleration due to gravity

α is Earth elasticity

M_λ, M_ϕ is depth-integrated momentum dispersion

E_{H_2} is horizontal eddy viscosity

$\tau_{s\lambda}$, $\tau_{s\phi}$ is applied free surface stress

τ_* is bottom stress

η is Newtonian tide potential

ADCIRC uses an unstructured, irregular mesh, consisting of triangular elements which allow the mesh to conform to a varied coastline. The size of mesh elements is allowed to vary over the domain so that greater detail may be established for areas requiring greater

resolution. Other static input data fields, such as bathymetry or coastal form, must be interpolated onto the mesh generated.

The domain of the mesh is bound in part to the coastline, and on the open ocean side a semi-circular arc is established such that the radial fetch in any ocean direction is roughly equal from the centrally located point of interest. A coastline was extracted from the intersection of the highest recorded water height in northern and western Alaska (4.0 m) with the bathymetry/topography data, rather than from linear, arc-based coastline data. This allows incorporation of nominally dry land within the domain, which enables a full surge runup solution. Tides are forced on the open ocean boundary using the five strongest tidal constituents for this region as specified in the LeProvost tidal database.

Once the domain is established the mesh must be carefully built. Proper element size is necessary for correct circulation simulation. If the elements are overly large there is not enough resolution to accurately determine water elevations. If they are too small the model is prone to numerical instability which can lead to runaway results. ADCIRC has a range monitor that traps for excessive water level heights and terminates the run in a controlled fashion. The nature of the wetting and drying response at the coastline interface is also specified.

The three primary inputs for surge simulation are bathymetry, wind velocity and atmospheric pressure. Bathymetry is interpolated onto the unstructured mesh and specified in the same input file describing the mesh. The grid is defined by node locations, node neighbors (elements) and boundaries. Wind velocity is specified on either a regular grid or on

the unstructured mesh on a specified time interval. The model calculates wind stress from wind velocity (equation 2.3) using Garratt's formula (Garratt, 1977) for drag co-efficient (equation 2.4).

$$\vec{ws} = C_d \cdot 0.001293 \cdot \vec{U} \cdot U \tag{2.3}$$

$$C_d = 0.001 \cdot (0.75 + 0.067 \cdot U) \tag{2.4}$$

where

ws is the wind stress

U is the 10 meter wind velocity

C_d is the drag coefficient

maximum C_d is 0.0003

Output from the model includes water surface elevation, depth averaged current velocity, wind velocity, and pressure. Recording stations may be designated at any grid point in the domain and set to record time series data for water level, current velocity and meteorological parameters.

2.2 Grid development

Using SMS, the bathymetric/topographic grid was built for the area of interest using data imported using data from the ETOPO1 Global Relief Model from the National Geophysical

Data Center (Amante and Eakins, 2009). ETOPO1 offers a resolution of one minute by one minute for the entire globe, combining data from disparate sources into a seamless dataset. To properly represent low lying areas potentially vulnerable to surge, measured coastline data was not used.

Data for the area of interest was extracted using the GEOphysical DAta System (GEODAS) Grid Translator and imported from plain XYZ format text files that use geographic coordinates with elevation in meters above mean sea level (negative is subaerial). The elevation data were reversed in sign so that positive values are depth below mean sea level, following the ADCIRC convention. The coordinate system was converted to Universal Transverse Mercator to allow distance calculations directly from the coordinates for use in unstructured grid creation.

Once the region of interest was selected, the coastline was edited to include only the relevant boundary. Boundary conditions were set for islands within the domain to allow transport across these areas. Selecting the encircling coastline segments, the domain was specified that includes a semicircular arc to enclose the open ocean boundary. Open ocean boundary nodes at the edge of the domain were set such that tidal components could be assigned at the nodes to allow tidal forcing to be transmitted into the domain.

Discussions with other ADCIRC modellers indicate that it is optimal to include deep ocean in the model domain (B. Blanton 2010, personal communication). With this in mind the domain was created to include as much open water as possible without including land on the far side of the Chukchi Sea.

The generation of the mesh took several factors into account. A calculation was performed to determine the shallow water wave wavelength. This value formed a starting point for an element size grid. This grid was then scaled as a function of the distance from the shoreline. A limit was placed on minimum possible size of any element. This served to limit numerical instability problems caused by overly small elements. Finally, internal consistency was verified by ensuring there were no abrupt changes between adjacent elements, and a mesh of elevation data was generated based on the size grid using a technique called scalar paving.

Scalar paving fills the domain with triangular elements using a three step procedure: first, equilateral triangles based on the vertices of the domain are created; second, overlapping regions are removed; and third, iteration until the desired element size is approximated. When the paving is complete the elements are checked for quality. Elements with very small or very large interior angles are said to be of low quality and are tagged for adjustment. Based on the tagged elements the mesh was then manually manipulated until element quality was satisfactory. The resultant mesh can be seen in figure 2.1.

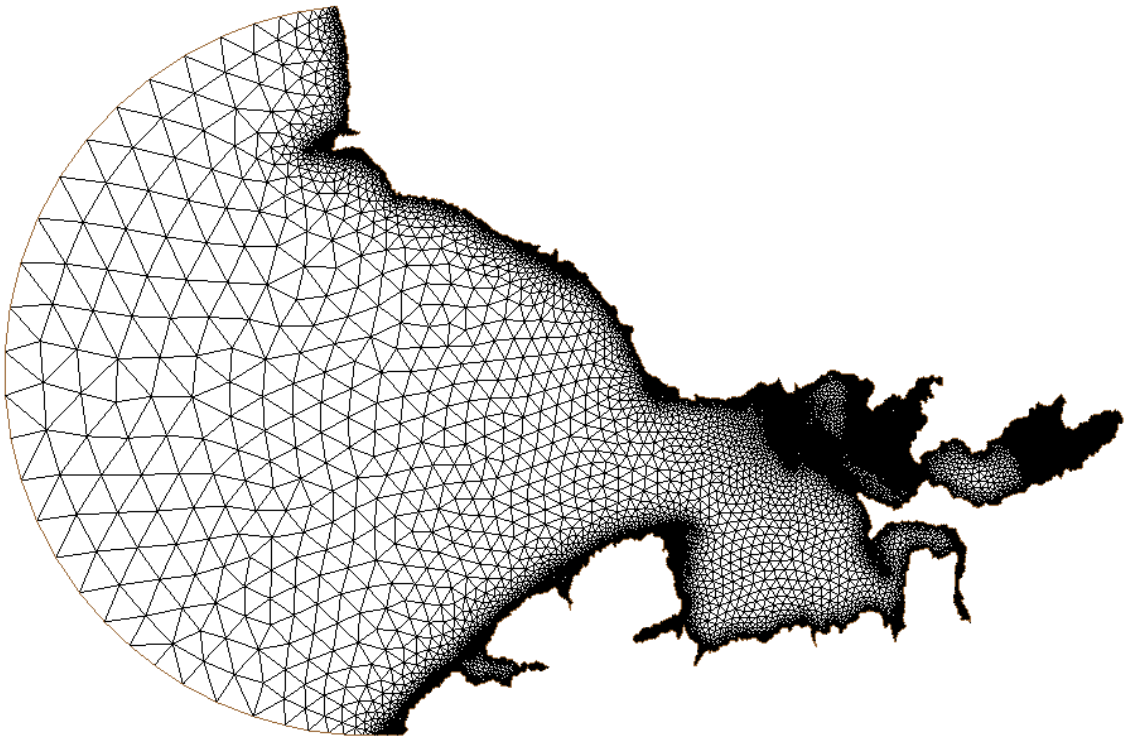

Figure 2.1. Unstructured finite element grid used in ADCIRC

The resolution of the ETOPO1 data set was not sufficient to represent certain topographical features deemed critical to the proper assessment of surge response. This required a second round of manual manipulation to ensure that they were well represented. This was necessary, for example, with the higher elevations (up to 20 m) found in the isthmus leading to the Baldwin Peninsula which is otherwise below the ETOPO1 spatial resolution. Without editing the automated smoothing process resulted in an assignment of very low relief in the isthmus which, during domain testing, resulted in unrealistic flooding across the isthmus and onto the peninsula itself. Editing of the elevation of these geographic features was performed manually using U.S. Geological Survey (USGS) topographic quadrangles as a reference.

2.3 Model forcing

2.3.1 Wind and pressure field

ADCIRC requires two meteorological parameters as input: winds at 10 m above ground and atmospheric pressure. These data fields were generated using the following procedure.

A program was developed using NCAR Command Language (NCL) to generate the necessary wind and pressure input files using idealized scenarios. The program takes as input the starting central pressure, pressure tendency, storm center starting position, heading and speed and creates a field of pressure stored in an array. From the central pressure to the background pressure, a spline fit was created to ramp the pressure down quickly near the storm's center and slowly towards the outer radius (see figure 2.2). This pressure field was

applied to an array of the size necessary to force the model. Each timestep the program moves the storm according to the set heading and speed, modifying the pressure field to have the spline gradient fit the new central pressure.

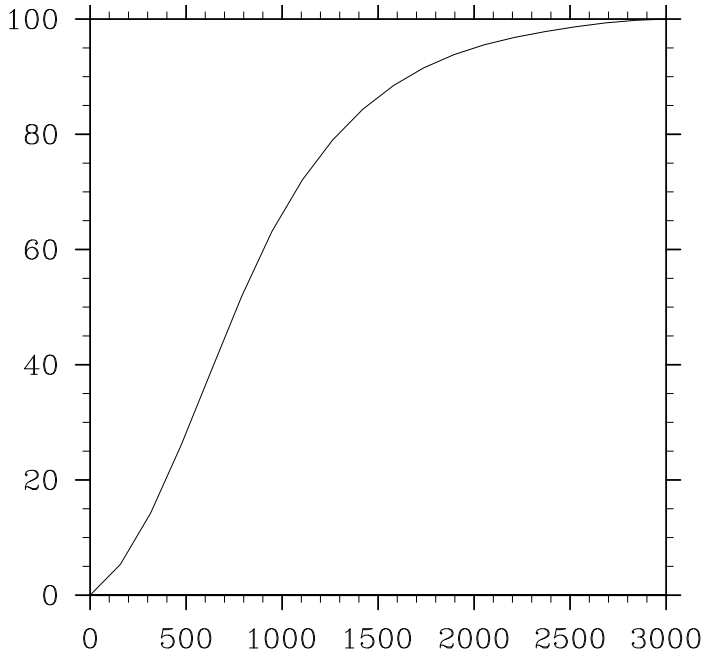

Figure 2.2. Spline curve of radial pressure variation. Percent of increase from storm central pressure to background pressure as a function of radial distance from the storm center in kilometers.

Using the quasi-geostrophic approximation 10 m vector wind components are generated for each time step using the pressure field. For the purposes of this study inputs were considered to be on a synoptic scale, so surface roughness and other local effects controlling wind were ignored. The resulting wind and pressure data were then fed directly into the ADCIRC model.

2.3.2 Storm track specification

Wind and pressure fields were dynamically specified along seven different "common" storm tracks. The storm tracks are summarized in table 2.1 and shown in figures 2.3 and 2.4. These storm tracks represent the most commonly observed paths of storms in western Alaska north of the Aleutian Islands.

The most common storm track pattern takes storms from the western North Pacific north-northwestward towards the Aleutian Islands. These often get their start off the east coast of Japan over the warm Kuroshio current or as Asian east coast baroclinic lows. Tropical cyclone remnants can also follow this path. While most storms proceed east to the Gulf of Alaska or the eastern North Pacific, another track takes some systems north into the Bering Sea (Rodionov et al., 2007). In the fall, the contrast of the cold pool of air over Siberia and the warmer air over the ocean provides energy to keep the storm going. On occasion the juxtaposition of a strong upper level trough can provide significant support to allow "explosive" re-energizing of a storm.

Powerful storms are also possible on the Arctic Ocean coast, for example the October 1963 (Hume and Schalk, 1967) and August 2000 cyclones (Lynch et al., 2003). These systems formed along the arctic front in Siberia, before moving northeast to the East Siberian Sea and intensifying due to convection. These storms typically then move into the central Arctic Ocean, but can be guided eastward by upper level steering.

For each track, two pressure patterns were considered: "moderate" and "strong". The moderate scenario dictated a constant pressure gradient throughout the storm's lifetime hav-

ing a geopotential height difference of 180 m and maximum winds around 15 m s^{-1}, while the strong scenario had a deepening pressure starting with a geopotential height difference of 120 m and decreasing by 60 m each day, with maximum winds approaching 30 m s^{-1}.

For each track and pressure scheme two storm ground track speeds were considered: 20 km/h and 30 km/h. The pressure pattern and ground track speeds are summarized in table 2.2. All storms were set to idle in place with constant central pressure for the first 24 hours in order to allow for tides and initial wind field setup to ramp up and become stable. In this paper, storms are referred to by abbreviations representing the strength and track speed, as per table 2.2.

Table 2.1. Storm track starting position and headings. Track name, latitude and longitude coordinate and heading in degrees clockwise from north.

Track	Latitude	Longitude	Heading
AE1	72N	170E	270
AE2	70N	170E	270
AW1	72N	140W	90
AW2	70N	140W	90
BS1	60N	172E	40
BS2	60N	176W	20
SEC	74N	170E	125

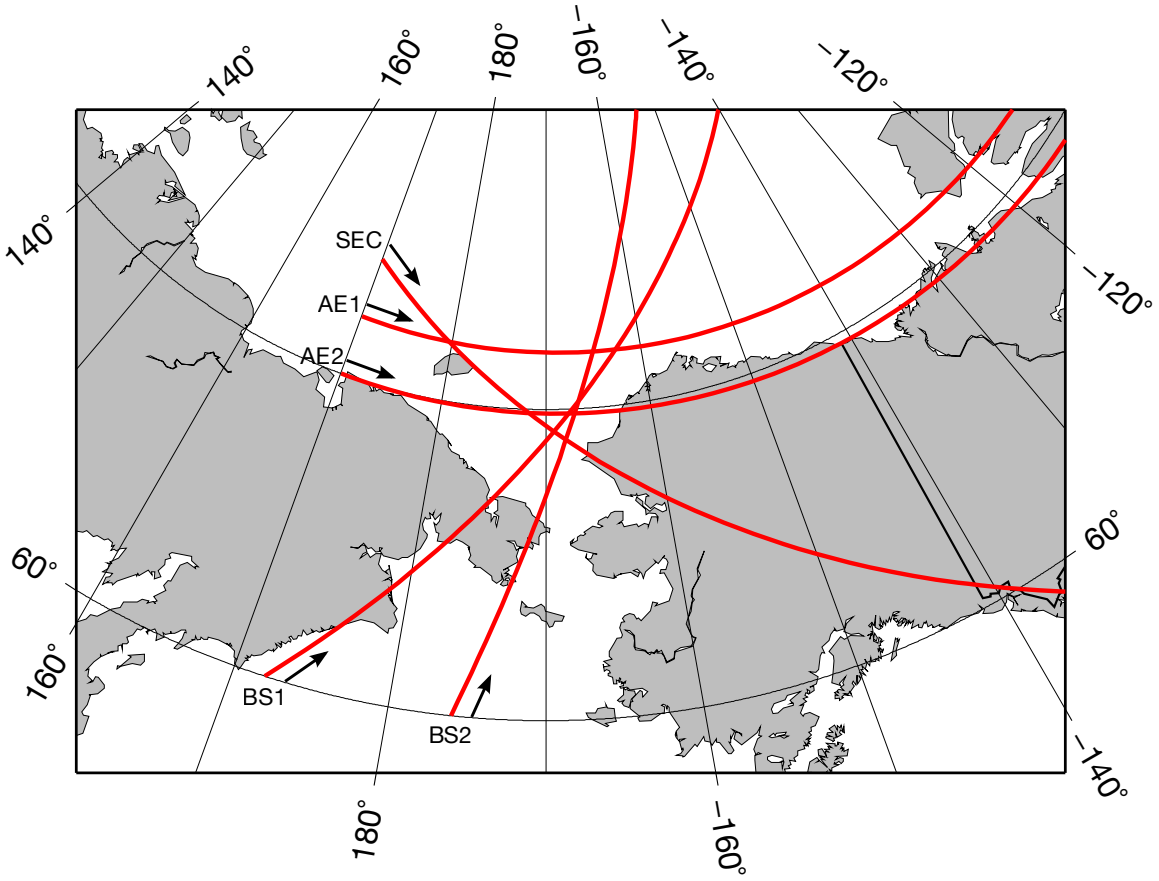

Figure 2.3. Map of storm tracks AE1, AE2, BS1, BS2 and SEC.

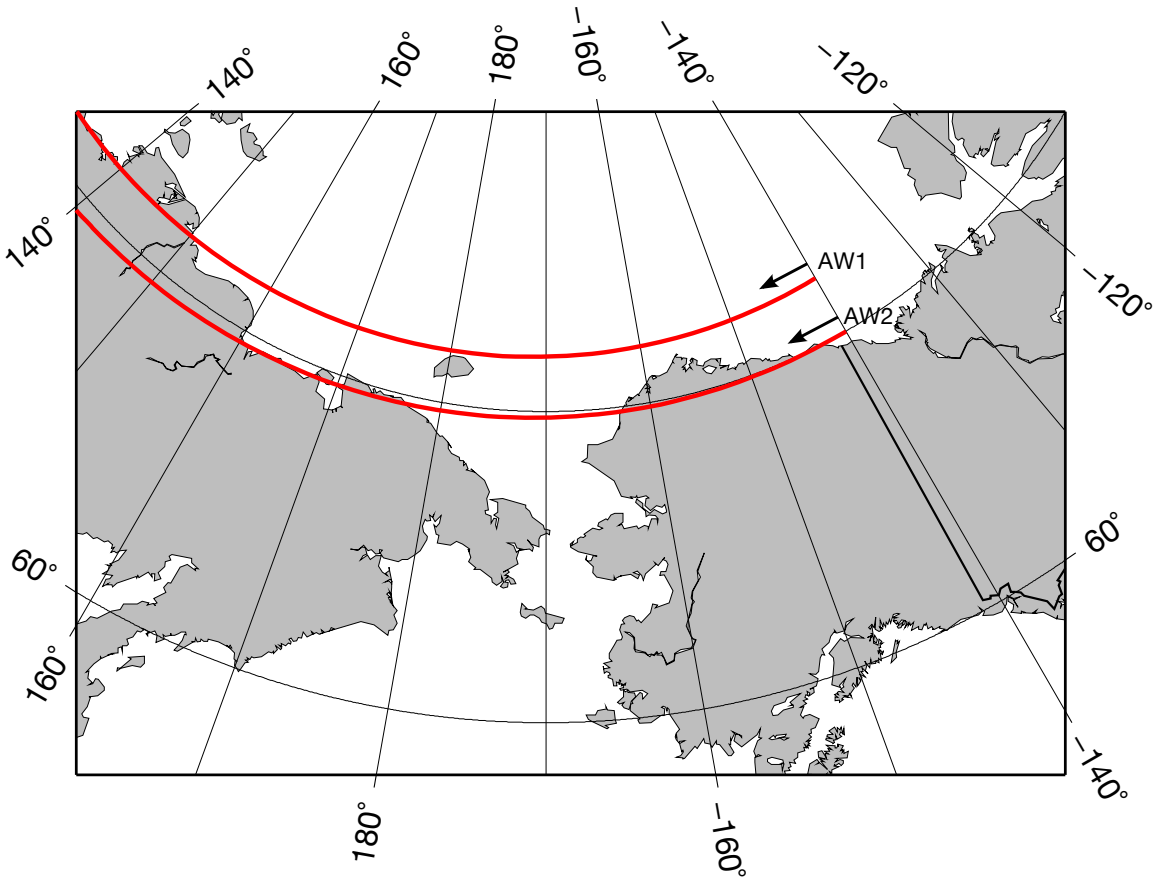

Figure 2.4. Map of storm tracks AW1 and AW2.

Table 2.2. Storm intensity and track speed by type

Storm type	Storm intensity	Track speed
MS	moderate	20 km/h
MF	moderate	30 km/h
SS	strong	20 km/h
SF	strong	30 km/h

Winds and pressure were input on a regular grid on a three hour time step. ADCIRC uses the equation 2.3 to calculate wind stress, and interpolates the wind stress and pressure data onto the irregular mesh and to the model time step.

2.4 Model operation

A number of parameters are set to be constant for all simulations performed. The coordinate system was set to spherical. All simulations begin with a cold start, where the model is not given any information about the state of water previous to the start time. The bottom friction term was set to varying quadratic, which means the frictional iteration between the ocean and the bottom are not constant but based on the elevation mesh and so varies with depth. Gravity was set to 9.81 m s^{-2}, which in turn specifies that other units are metric. Wetting and drying was enabled, allowing persistently dry areas to be treated as such and flooding to occur on areas otherwise above water. The GWCE weighting factor, τ_0, was set to 0.01. This factor weighs the relative contribution of the primitive and wave portions of the GWCE.

Five tidal constituents were forced along the open ocean boundary, K1, M2, N2, O1, and S2. These constituents make up the majority of the tidal signal. Tides are generally weak in the area of study; see table 2.3 for tidal constituent amplitudes.

Table 2.3. Tidal constituents used and their amplitudes at Red Dog Dock. Amplitudes are one-half of the range of tidal constituents and are specified in meters. From NOAA Tides and Currents.

Name	Type	Amplitude
M2	princial lunar	0.074
K1	luni-solar declinational	0.021
N2	elliptical lunar	0.018
O1	principal lunar declinational	0.010
S2	principal solar	0.014

Selection of an appropriate time step is critical to the operation of any finite element model. Too short and runs consume unnecessary amounts of CPU time; too coarse and model runs can suffer from numerical instabilities. A convenient metric to guide time step selection is the Courant number, which is defined as

$$C = \frac{\Delta t \sqrt{gh}}{\Delta x} \tag{2.5}$$

where

g is the acceleration due to gravity

h is the nodal depth

Δt is the time step

Δx is the nodal spacing

A starting point that optimizes both model stability and accuracy of results stipulates that the Courant number should not exceed unity (Westerink et al., 2008). Proceeding from this, through trial and error a time step of five seconds was decided upon for all experiments with assistance from Brian Blanton (2010, personal communication).

Initial model testing runs revealed a number of modifications that needed to be made. Element size was increased and timestep decreased to prevent instability. The run time was increased to allow for storms to reach their peak and begin a decline within the allotted time.

Simulations were performed on nodes at the Arctic Region Supercomputer Center (ARSC). An individual simulation run of 7 days with a time step of five seconds took approximately four hours to compute. Multiple, simultaneous simulations were possible across multiple nodes; true multi-threading was not enabled for this project.

2.5 Observational comparison

For comparison of modeled results to real world storm surge in the area, six minute water level data was obtained for the NOAA National Ocean Service water level recording station at Red Dog Dock. For consistency with the model data set, the mean sea level datum was used. Data for June 30, 2004 (the start of operation of the station) to December 31, 2009 were studied. Dates where storm surge (verified tide gauge water level measurement minus

predicted tide level) exceeded 1 m were found and each date or cluster of contiguous dates were treated as events. Daily composite charts from the NCEP/NCAR Reanalysis (Kalnay et al., 1996) were analyzed to assess the meteorological pattern for each event.

Chapter 3

Results

Refer to figure 3.1 for place names in the Kotzebue Sound area. For the purposes of this section, upsound refers to movement in the direction of Kotzebue. The wind direction convention is a meteorological one, where directions refer to where the wind is blowing from. Storm types refer to designations given in table 2.2.

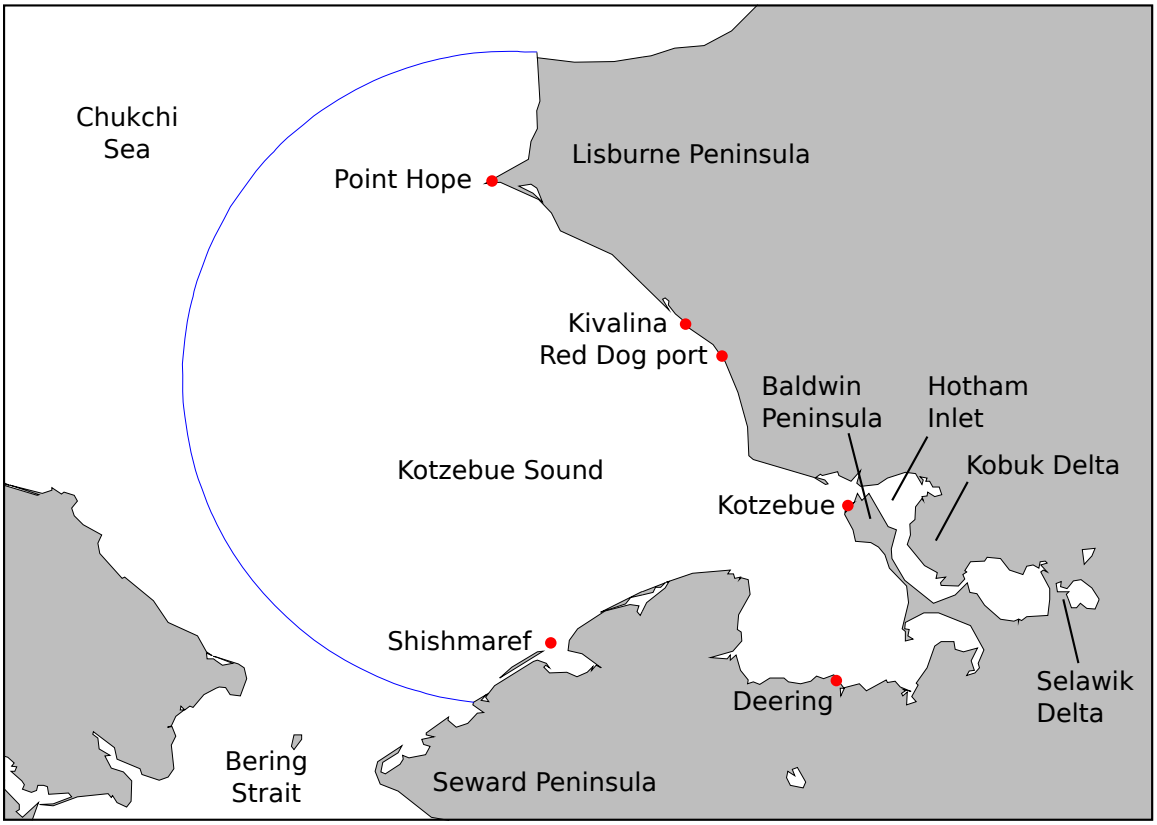

Figure 3.1. Map of Kotzebue Sound region. Recording stations are located adjacent to marked settlements. Blue line indicates open ocean boundary of ADCIRC grid.

3.1 Model results

3.1.1 Track AE1: North coast, eastward propagation, 70N

In the first scenario, AE1, a storm passes along the north arctic coast in an eastward direction starting from the East Siberian Sea at 72N 170E. As a low pressure system in the Northern Hemisphere, winds around the storm are counterclockwise. As the storm center crosses over the middle of the Chukchi Sea its wind pattern is lined up such that the wind is southwesterly, in the direction of Lisburne Peninsula, and then veer to point southeast, in the direction of inner Kotzebue Sound.

MS and MF storms produced a noticeable surge in eastern parts of Kotzebue Sound, in excess of double the tidal signal for both storm ground track speeds. It was apparent from the winds, however, that there is enough distance from the storm such that, when the winds shift to northwesterly that the wind speed is already past peak, decreasing the duration of winds in the upsound direction and so reducing surge response. SS storms generated a much greater surge (peak water level shown in figure 3.2), measuring around 1.0 m in the Kotzebue area (figure 3.3) and 1.3 m near Deering for the 20 km/h storm.

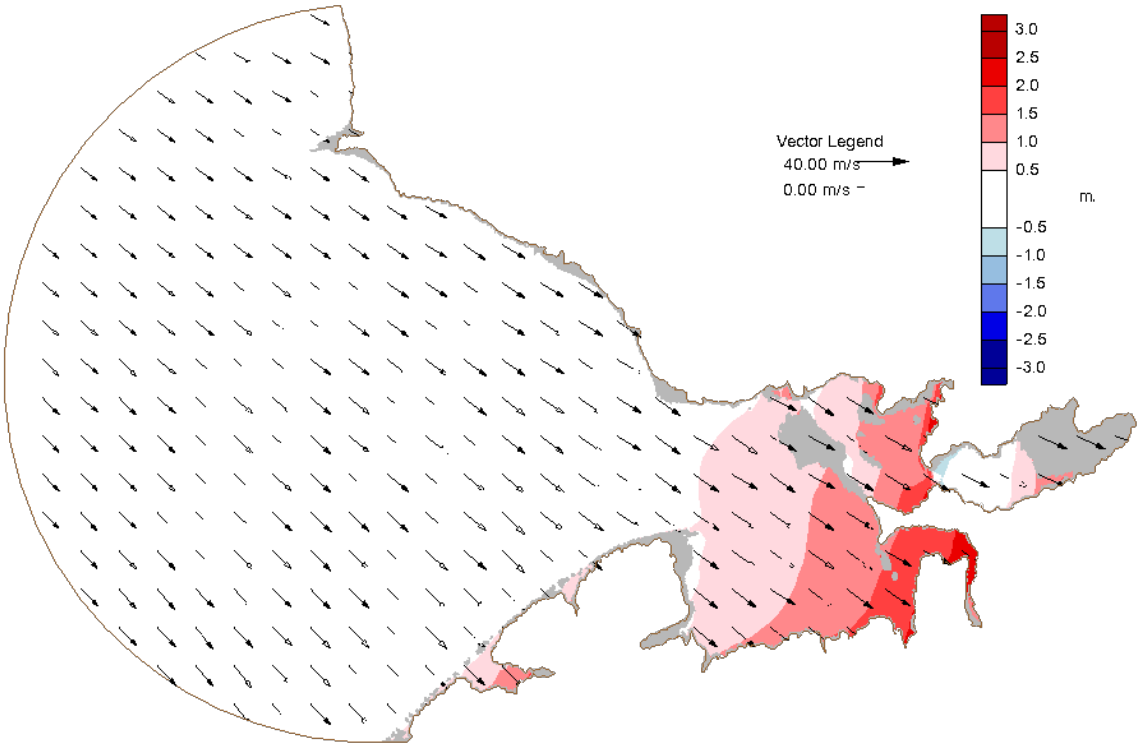

Figure 3.2. Winds and water elevation for track AE1 SS at 84 hours. Color filled contours are water elevation in meters relative to mean sea level with areas in gray indicating dry land within the domain. Vectors are 10 m wind velocity displayed on a constant grid.

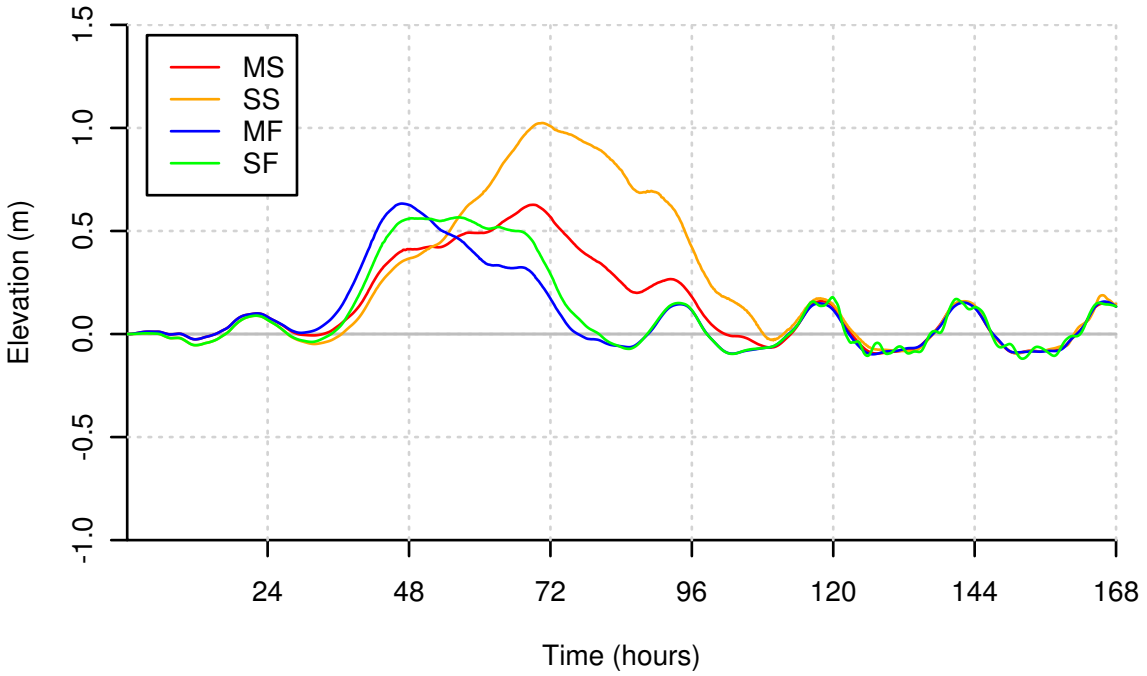

Figure 3.3. Time series of water elevation at Kotzebue for track AE1. Elevation in meters relative to mean sea level.

In contrast, the faster SF storm showed a noticeably weaker surge, producing water elevations closer to 0.6 m around Kotzebue.

Flooding of the otherwise dry areas of the Kobuk and Selawik river deltas occurred for all events (figure 3.4). The Kobuk delta saw flooding of magnitudes similar to those observed near Kotzebue, however peaking around 24 hours later. Unlike Kotzebue, in this case there was no tide signal evident and the high waters took much longer to dissipate. That is, west of the Baldwin Peninsula the waters returned to pre-flood levels 36 hours after reaching a peak, east of the peninsula it took nearly 72 hours.

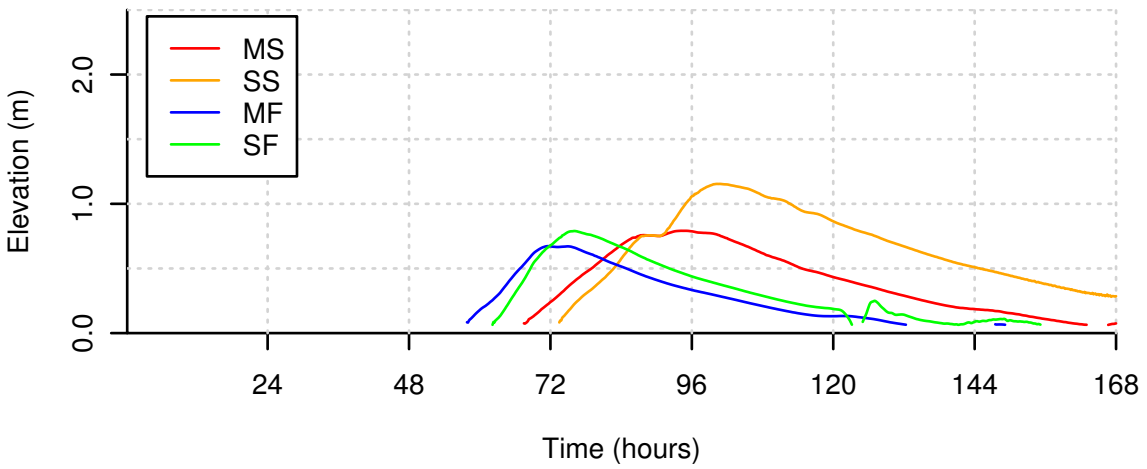

Figure 3.4. Time series of elevation in the Kobuk delta for track AE1. Elevation in meters relative to mean sea level.

Outer areas of the sound saw less surge. On the southern Lisburne Peninsula, water levels at Kivalina rose to less than 0.4 m before the wind shift (figure 3.5). On the outer Seward Peninsula coast, water levels at Shishmaref reached 0.4 m at most (figure 3.6).

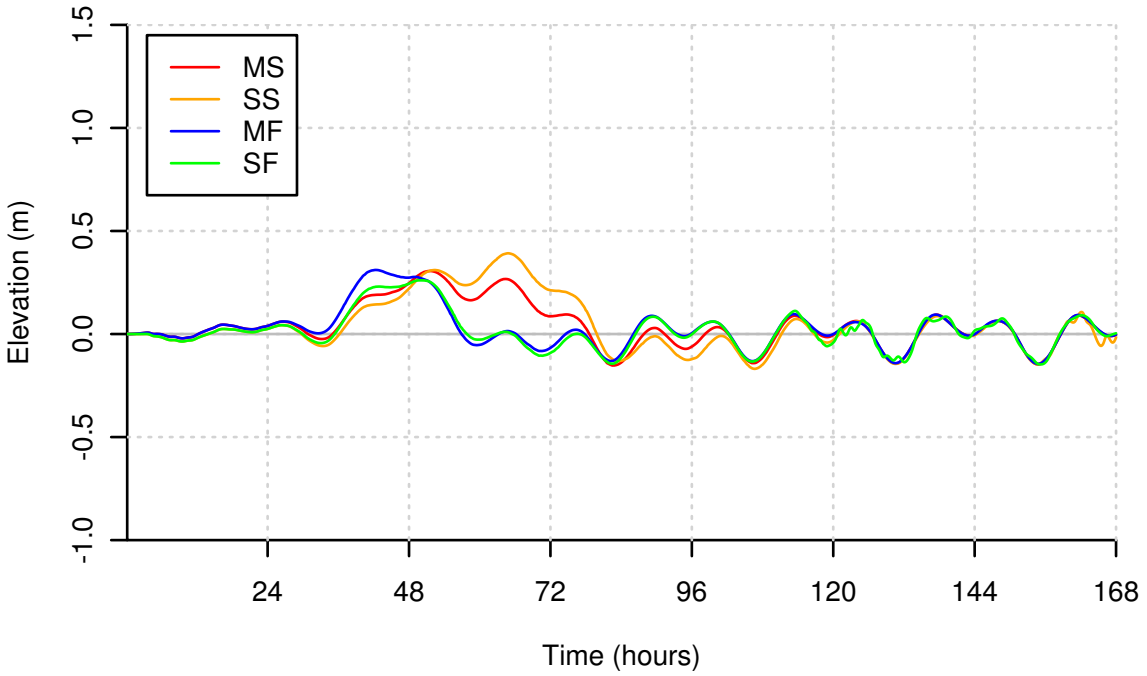

Figure 3.5. Time series of water elevation at Kivalina for track AE1. Elevation in meters relative to mean sea level.

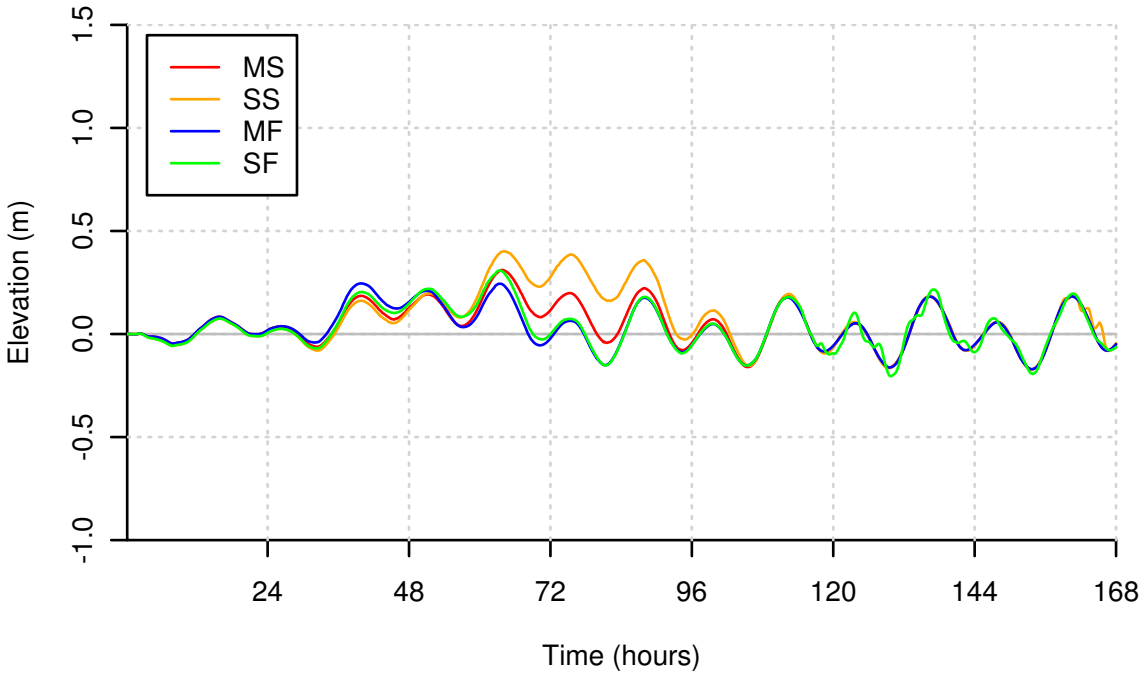

Figure 3.6. Time series of water elevation at Shishmaref for track AE1. Elevation in meters relative to mean sea level.

3.1.2 Track AE2: North coast, eastward propagation, 68N

The second storm track, AE2, is similar to the first except starting at 2 degrees more southerly latitude. Wind directions were more sharply meridional with this track, starting south-southwesterly becoming north-northwesterly.

Owing to the more southerly winds, the outer Lisburne Peninsula coast saw higher water than in AE1 before the wind shift, followed by a weak negative surge. Peak water level is shown in figure 3.7. Despite somewhat stronger wind speeds, eastern Kotzebue Sound had lower water levels (figure 3.8), owing to the lack of an extended zonal component to the forcing. The southern portion of the sound however saw much higher water; Deering reported 1.8 m at the highest (figure 3.9), as contrasted with the 1.3 m maximum for AE1.

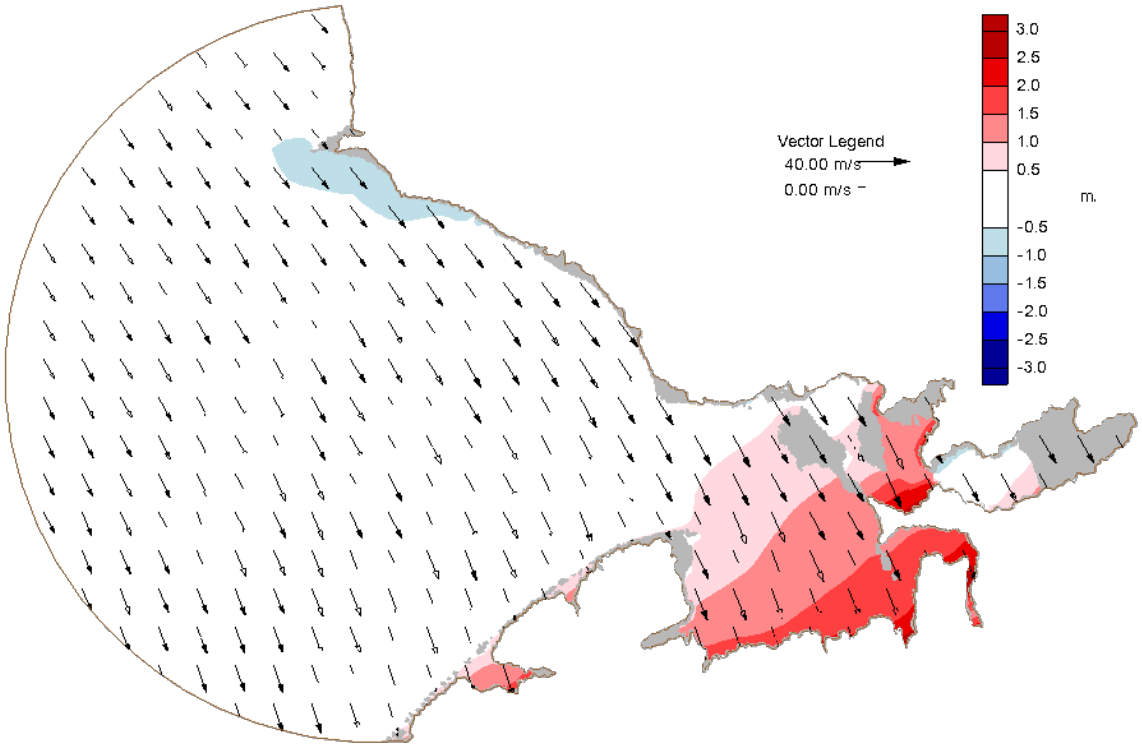

Figure 3.7. Winds and water elevation for track AE2 SS at 96 hours. Color filled contours are water elevation in meters relative to mean sea level with areas in gray indicating dry land within the domain. Vectors are 10 m wind velocity displayed on a constant grid.

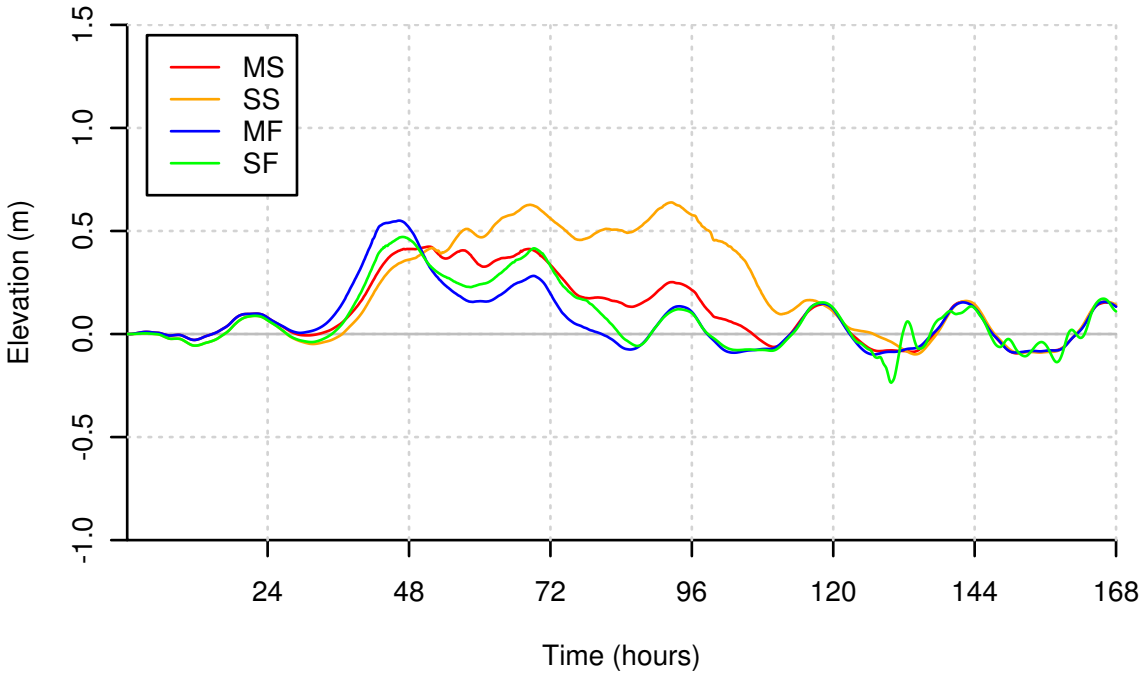

Figure 3.8. Time series of water elevation at Kotzebue for track AE2. Elevation in meters relative to mean sea level.

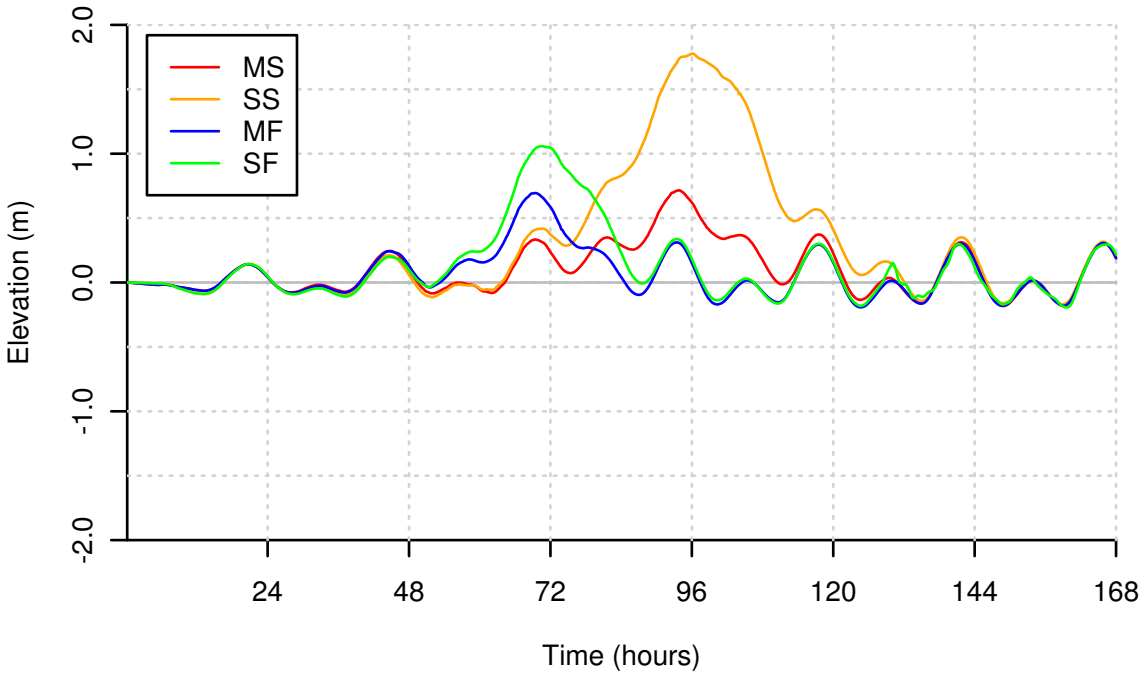

Figure 3.9. Time series of water elevation at Deering for track AE2. Elevation in meters relative to mean sea level.

3.1.3 Track AW1: North coast, westward propagation, 70N

Track AW1 follows the opposite direction of the first two scenarios. Starting at 72N 140W, north of the US-Canada border in the Beaufort Sea, the storm heads in a westerly direction along the line of latitude.

As the storm begins east of Chukchi Sea winds are northwesterly, before backing to southwesterly between hour 40 and 96 as the storm passes north of Kotzebue Sound for the slow storms; between hour 30 and 70 for the fast storms. Peak water level is shown in figure 3.10. At Kotzebue this is during the wind shift (figure 3.11), reaching 1.1 m (SS). On the southern Lisburne Peninsula, Kivalina and Red Dog Dock saw higher surge than with storms starting in the west (0.7 m compared to 0.4 m for SS at Kivalina; figure 3.12).

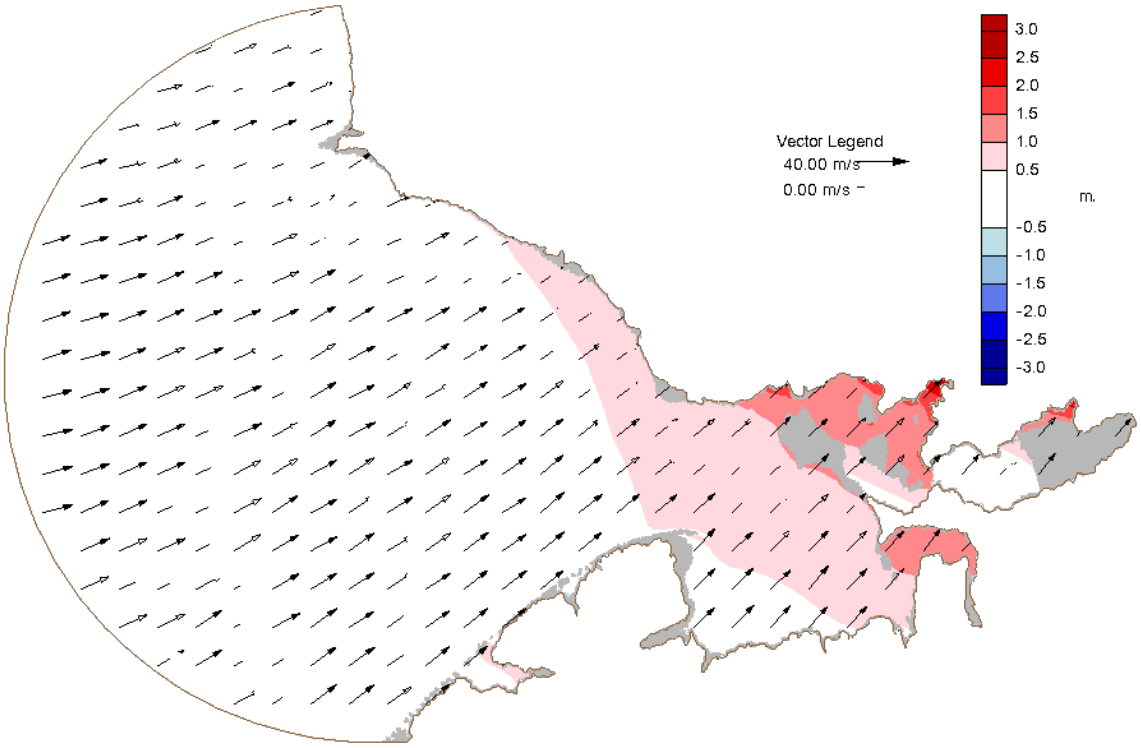

Figure 3.10. Winds and water elevation for track AW1 SS at 84 hours. Color filled contours are water elevation in meters relative to mean sea level with areas in gray indicating dry land within the domain. Vectors are 10 m wind velocity displayed on a constant grid.

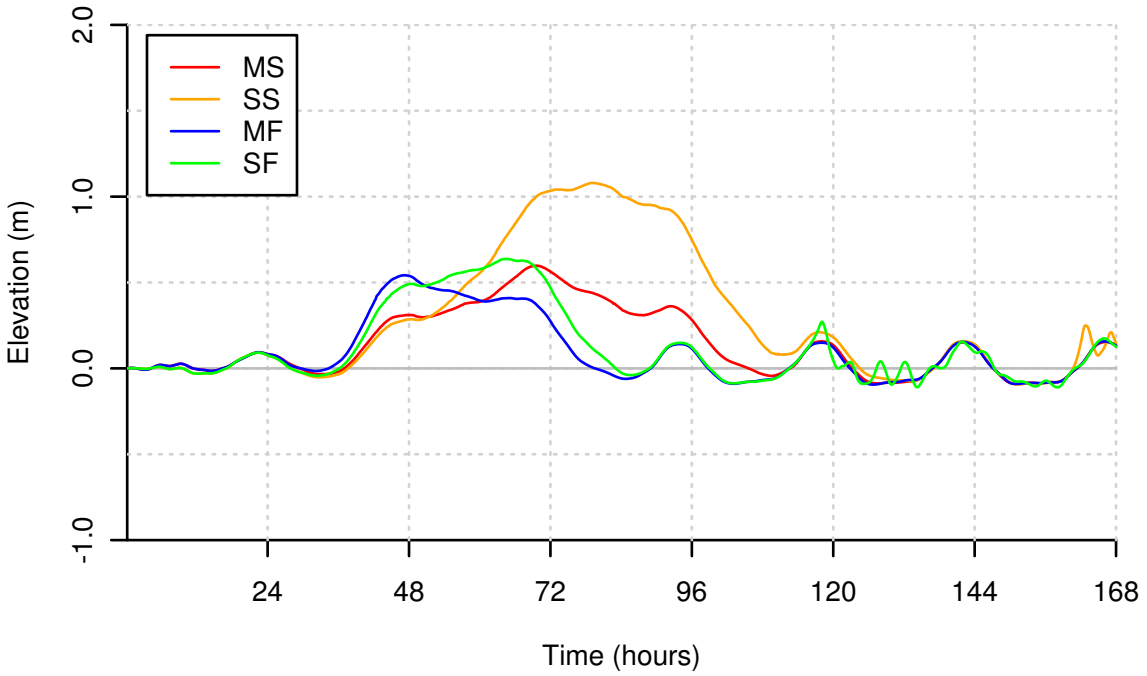

Figure 3.11. Time series of water elevation at Kotzebue for track AW1. Elevation in meters relative to mean sea level.

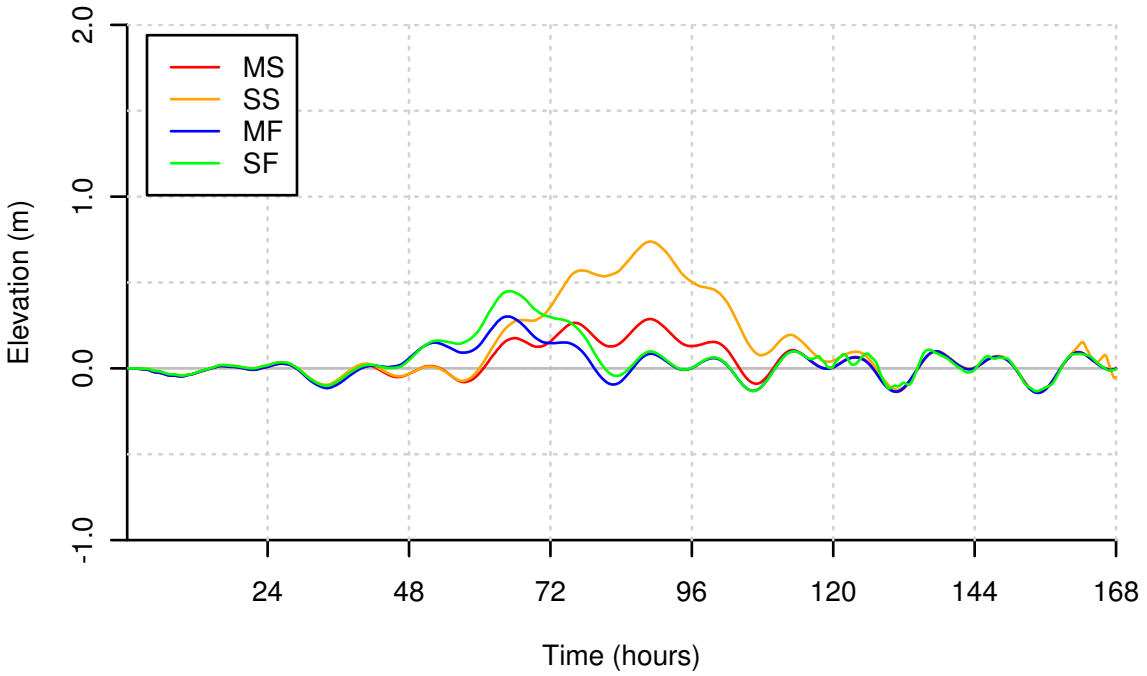

Figure 3.12. Time series of water elevation at Kivalina for track AW1. Elevation in meters relative to mean sea level.

Areas of the Kobuk Delta flooded starting early in storms' life cycles, staying below 0.3 m until ramping up to a peak of 0.8 m for SS at hour 96, and 0.5 m for other storms (figure 3.13). The peak flooding in Hotham Inlet lagged behind the peak water level at Kotzebue by 24 hours.

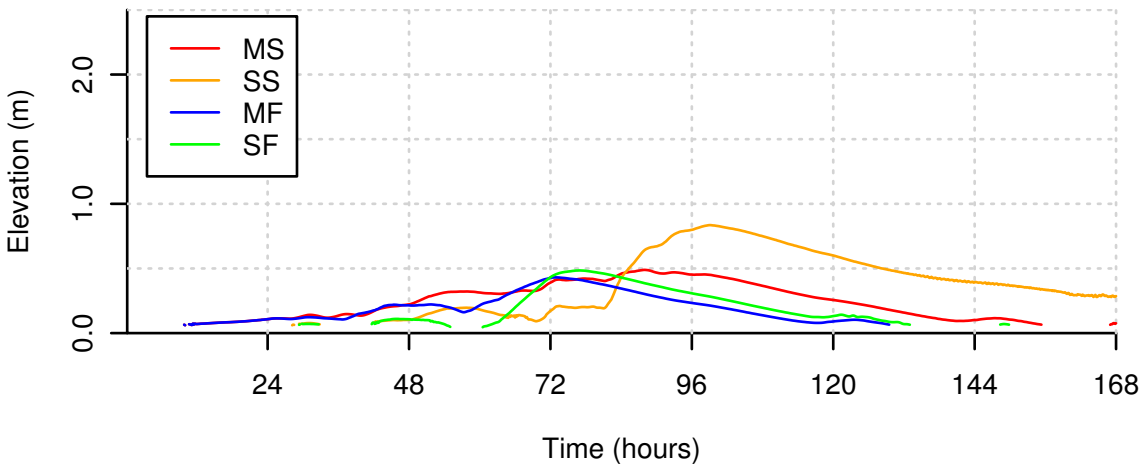

Figure 3.13. Time series of water elevation in the Kobuk delta for track AW1. Elevation in meters relative to mean sea level.

3.1.4 Track AW2: North coast, westward propagation, 68N

Track AW2 follows a westerly path from the Beaufort Sea similar to AW1, but at 2 degrees more southerly latitude.

Winds were more meridional in this scenario than in AW1, starting north-northwesterly and backing to south-southwesterly. This prevented water from reaching deeper within the sound, but caused more pronounced surge along the Lisburne Peninsula coast (peak shown in figure 3.14). Kobuk Delta and Deering both saw elevations 0.2 m lower than AW1 in strong storms, and nearly equal elevations in moderate storms. Meanwhile Kivalina, Red Dog and Point Hope saw higher higher elevations in all circumstances. For SS storms, Kivalina and Red Dog reached 1.1 m and 1.2 m respectively (figure 3.15), versus 0.7 m and 0.8 m for the same scenarios with track AW1.

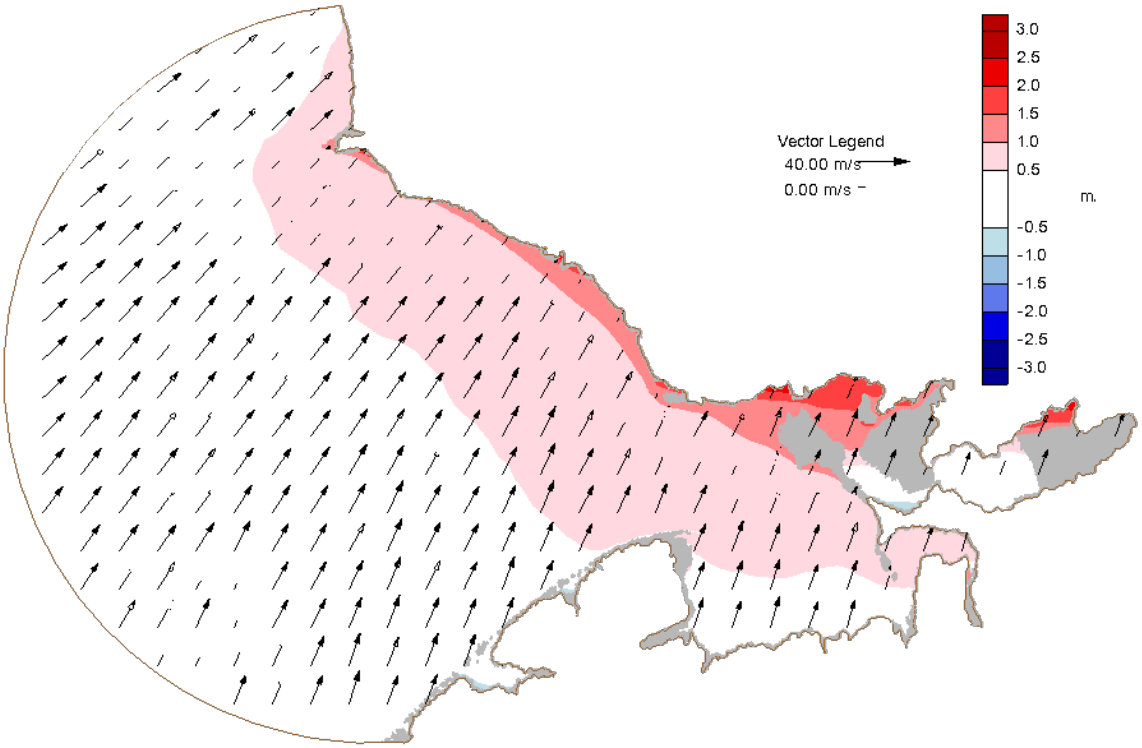

Figure 3.14. Winds and water elevation for track AW2 SS at 96 hours. Color filled contours are water elevation in meters relative to mean sea level with areas in gray indicating dry land within the domain. Vectors are 10 m wind velocity displayed on a constant grid.

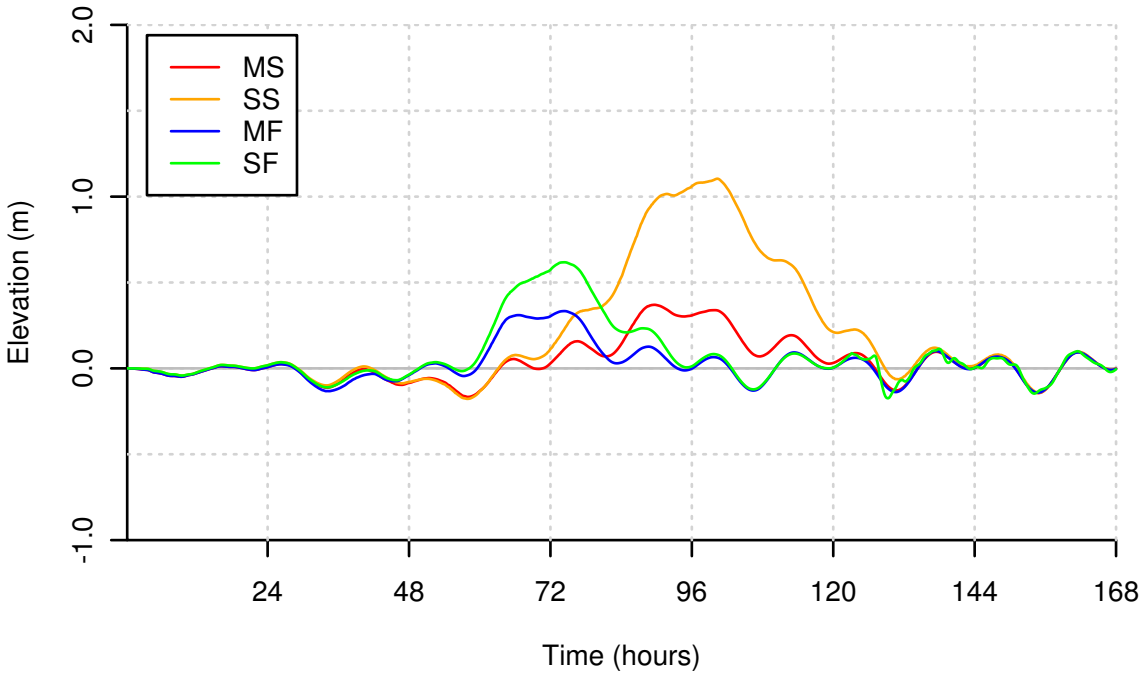

Figure 3.15. Time series of water elevation at Kivalina for track AW2. Elevation in meters relative to mean sea level.

3.1.5 Track BS1: Bering Sea, northeast propagation

The next two storms start in the Bering Sea, a more common path for storms affecting the Alaskan west coast. BS1 begins at 60N 172E in the far western Bering Sea and tracks a northwestern course through the Bering Strait into the Chukchi Sea.

Winds begin south-southeasterly, veering to west-northwesterly between hour 60 and 110 for slow storms; between hour 42 and 84 for fast storms. Winds peak near the end of the rotation. This appears to take full advantage of the funneling effect of the sound, with upsound winds causing high surge in many areas of the eastern end of the sound (peak shown in figure 3.16). At Kotzebue the water level reached a peak of 2.4 m at the highest (figure 3.17), while at Deering it reached 2.6 m. Outer areas saw roughly half

of this amount, but still significant surge with up to 1.0 m at Red Dog port and 0.9 m at Shishmaref.

The much higher surge for SS and SF for this track may be due in part to storm reaching the area of interest later in the storm life cycle when the storm has intensified. Surge for MS and MF are more comparable in magnitude to those of the previous tracks.

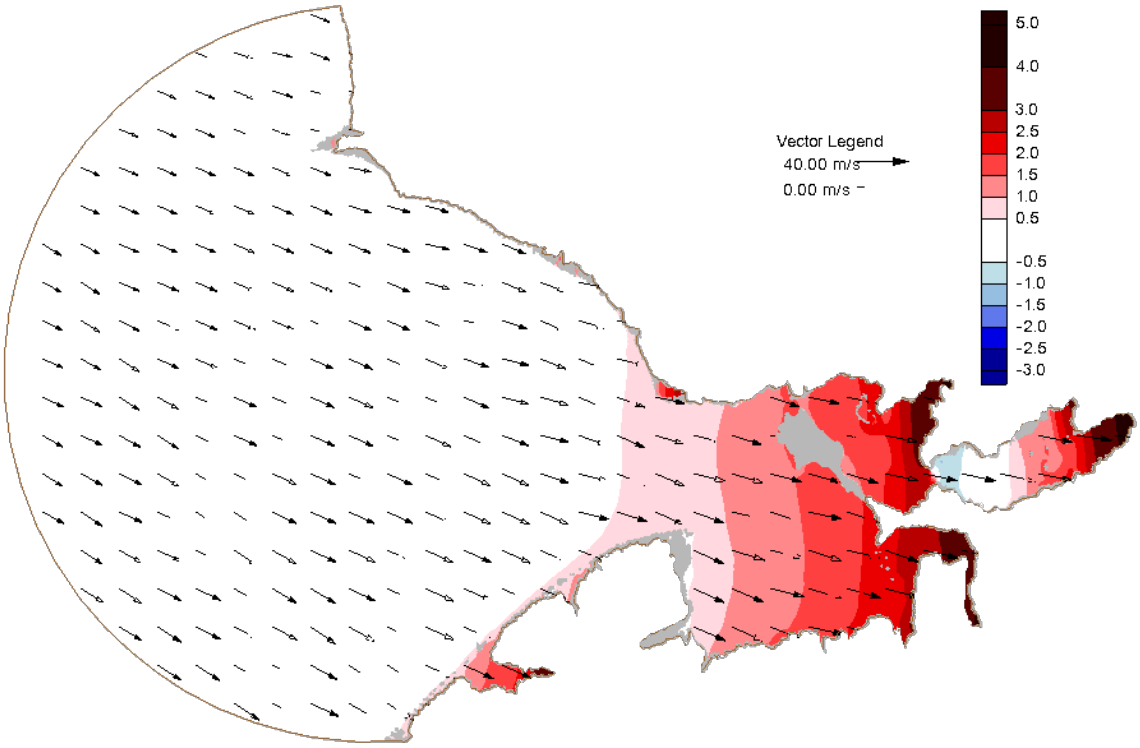

Figure 3.16. Winds and water elevation for track BS1 SS at 126 hours. Color filled contours are water elevation in meters relative to mean sea level with areas in gray indicating dry land within the domain. Vectors are 10 m wind velocity displayed on a constant grid.

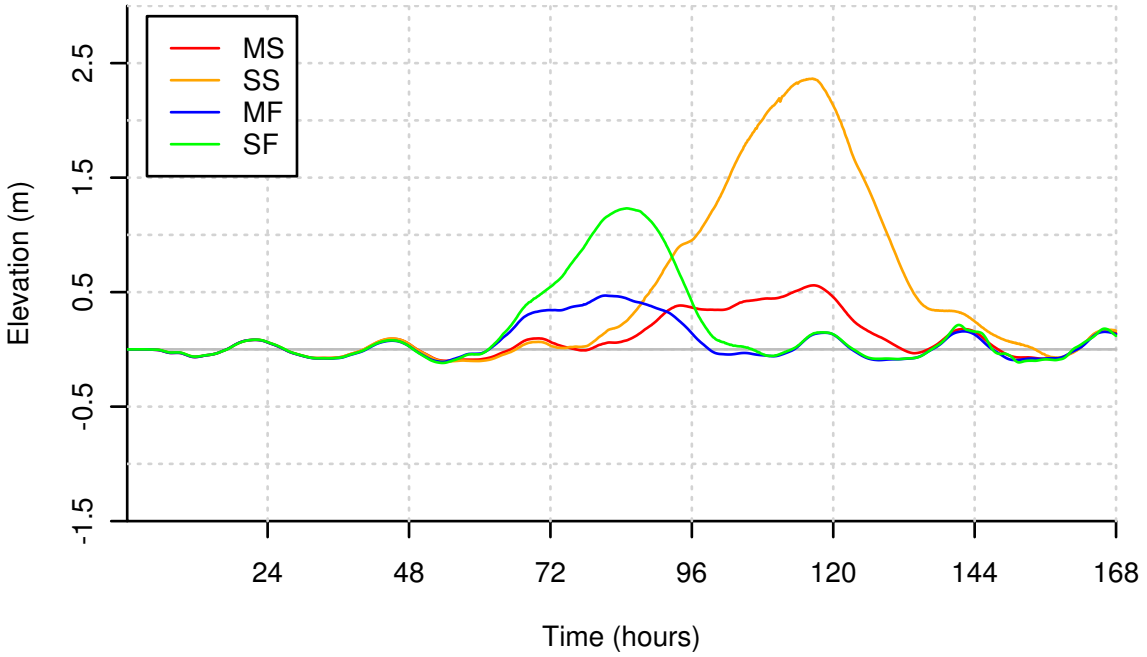

Figure 3.17. Time series of water elevation at Kotzebue for track BS1. Elevation in meters relative to mean sea level.

The delta region east of Baldwin Peninsula flooded quickly after waters at Kotzebue peaked and winds reached a westerly direction. The Kobuk delta went from dry to 1.7 m (SS) within 10 hours (figure 3.18). Dissipation of flood waters was again relatively slow.

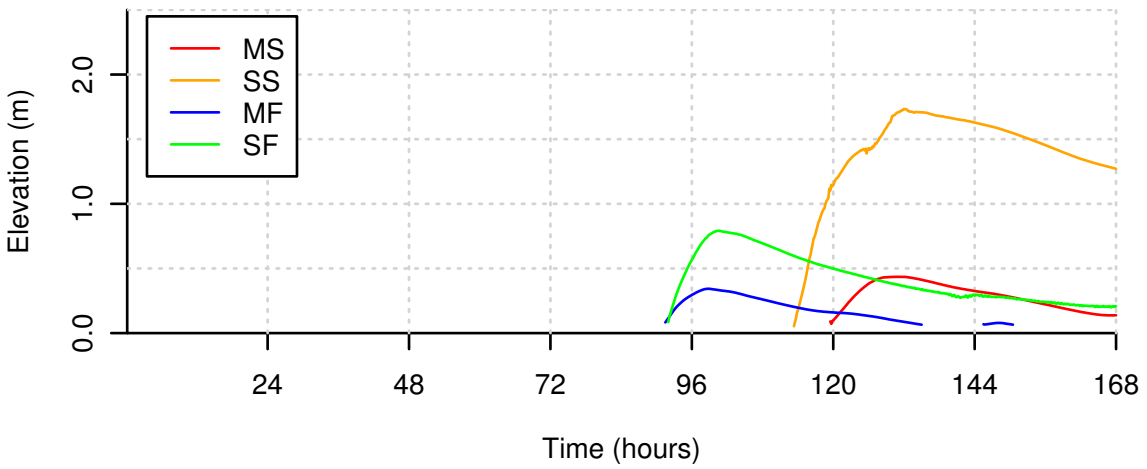

Figure 3.18. Time series of water elevation in the Kobuk delta for track BS1. Elevation in meters relative to mean sea level.

With nearly southerly winds for the before the wind shift, Deering saw water levels drop over 1 m before peaking at 2.6 m following the wind shift (figure 3.19).

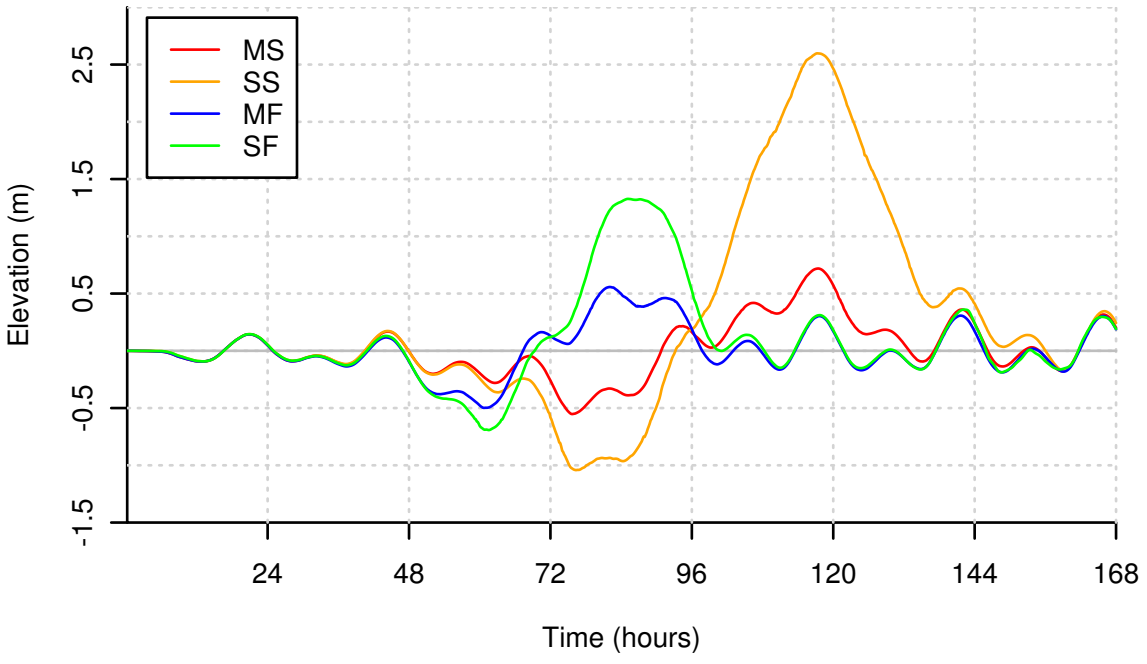

Figure 3.19. Time series of water elevation at Deering for track BS1. Elevation in meters relative to mean sea level.

3.1.6 Track BS2: Bering Sea, north-northeast propagation

Track BS2 starts in the central Bering Sea at 60N 176W and tracks in a more northerly direction that the previous storm at 20° east of north.

Winds begin east-southeasterly and veered around to nearly westerly. The easterly winds pulled water out of the sound, leading to negative surges in the eastern end of the sound (figure 3.20). Kotzebue reached -0.6 m while Deering reached -1.1 m. Following the wind shift, the sound rebounded to an even greater positive surge (figure 3.21), with the aforementioned sites reaching 2.0 m and 1.9 m respectively (figures 3.22 and 3.23).

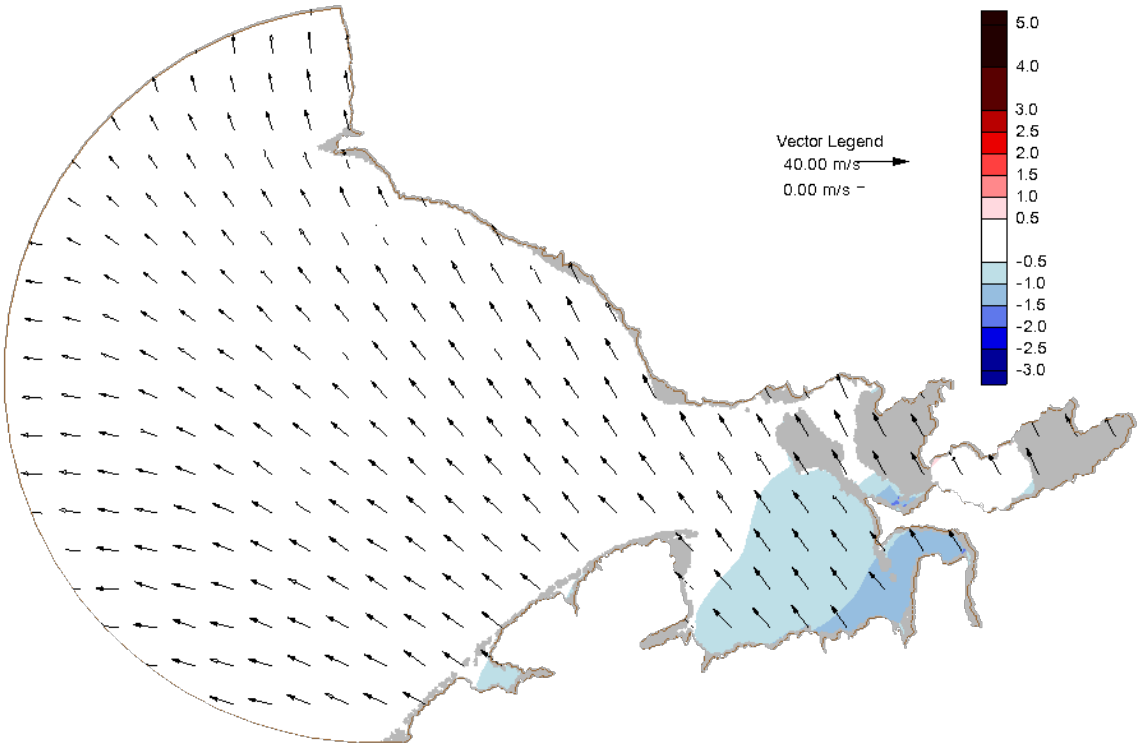

Figure 3.20. Winds and water elevation for track BS2 SS at 66 hours. Color filled contours are water elevation in meters relative to mean sea level with areas in gray indicating dry land within the domain. Vectors are 10 m wind velocity displayed on a constant grid.

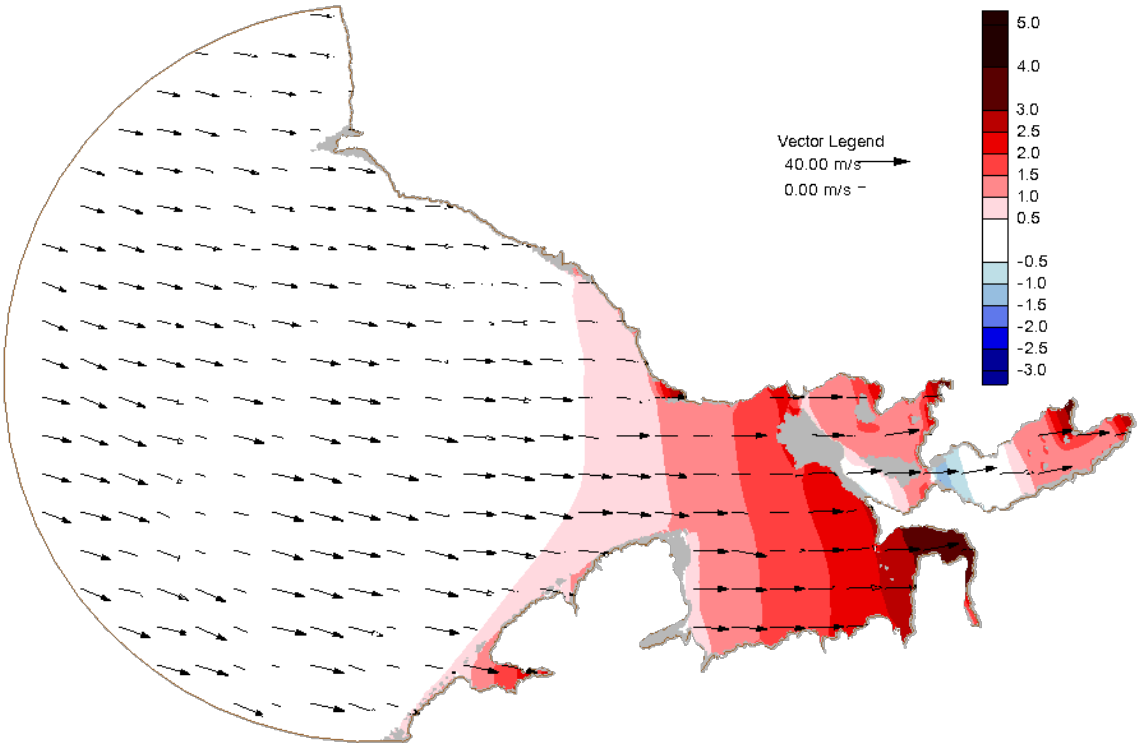

Figure 3.21. Winds and water elevation for track BS2 SS at 108 hours. Color filled contours are water elevation in meters relative to mean sea level with areas in gray indicating dry land within the domain. Vectors are 10 m wind velocity displayed on a constant grid.

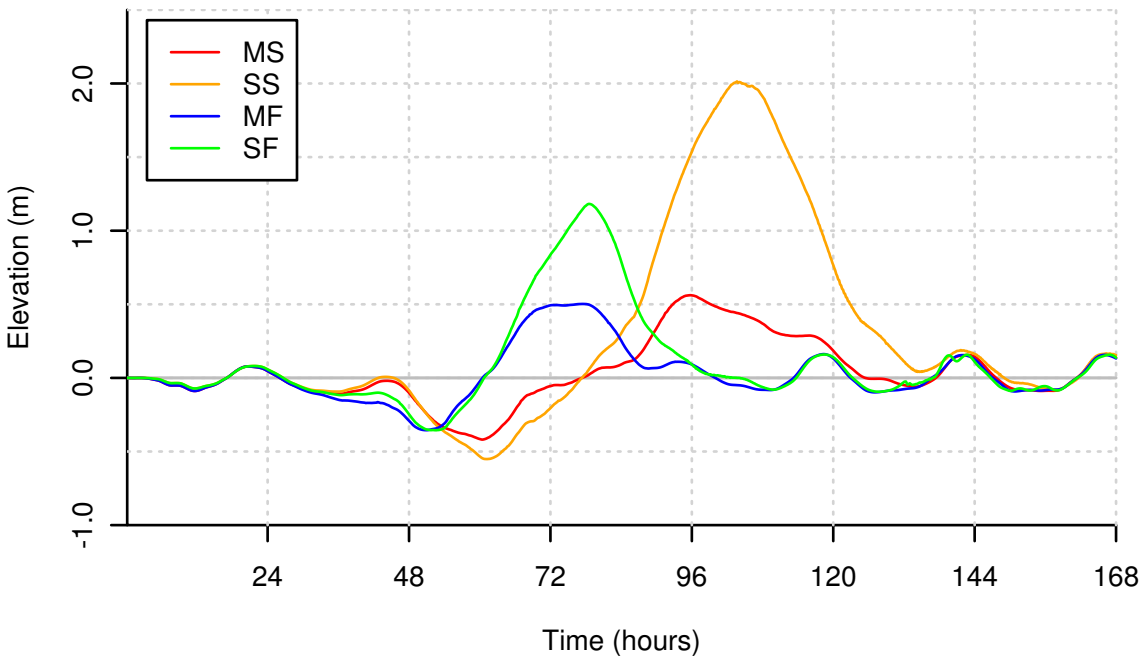

Figure 3.22. Time series of water elevation at Kotzebue for track BS2. Elevation in meters relative to mean sea level.

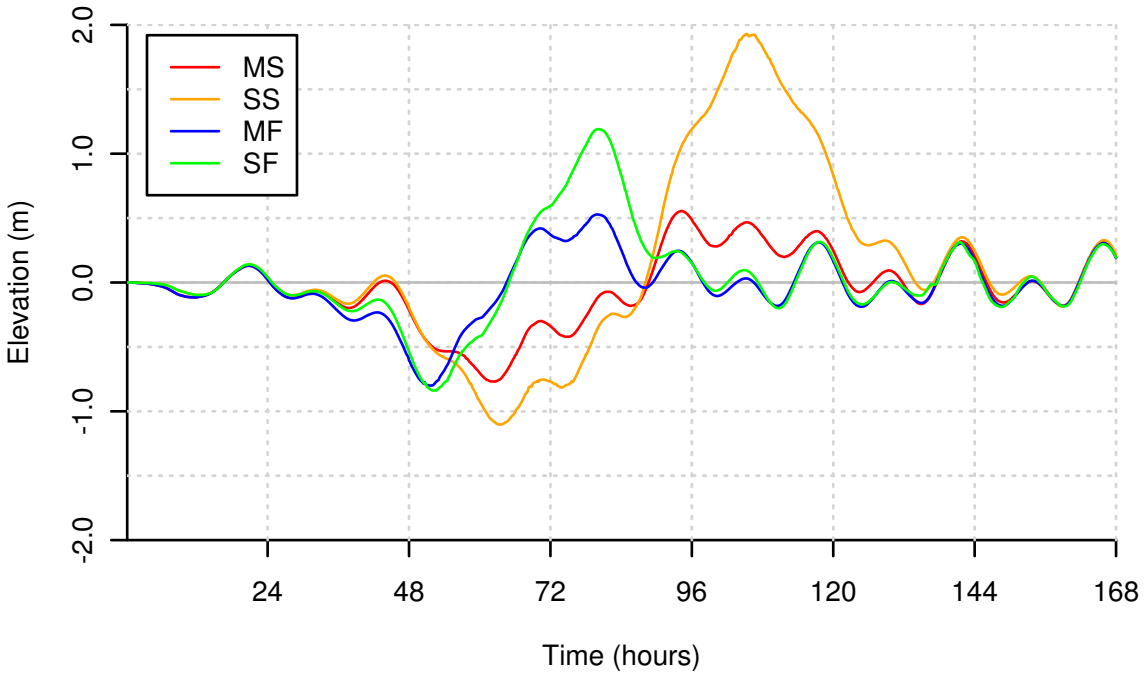

Figure 3.23. Time series of water elevation at Deering for track BS2. Elevation in meters relative to mean sea level.

3.1.7 Track SEC: cross Chukchi Sea, southeast propagation

Finally track SEC starts in the East Siberian Sea at 74N 170E in the high arctic and dives southeasterly through the central and southern Chukchi Sea intersecting the Lisburne Peninsula and onward into Interior Alaska.

Wind speeds reach a first peak while the winds are south-southwesterly, reach a minimum during the wind shift before a second, stronger peak after the wind reaches north-northeasterly. The center of the storm passes close to the domain so the wind shift is faster than that seen in other tracks.

Kotzebue Sound had a positive surge in areas followed by a more widespread and stronger negative surge (peak of negative surge show in figure 3.24). At Kotzebue there

is a moderate positive surge before the wind shift, followed by a strong negative surge (figure 3.25). For SF the water level falls below -1.7 m, causing the model to call the area dry. The area recovers back to tidal levels within 24 hours. A similar pattern is seen on the northern side of the sound with Kivalina and Red Dog reaching 0.5 m and 0.6 m before falling to -1.2 m and -1.4 m respectively for the same storm scenario.

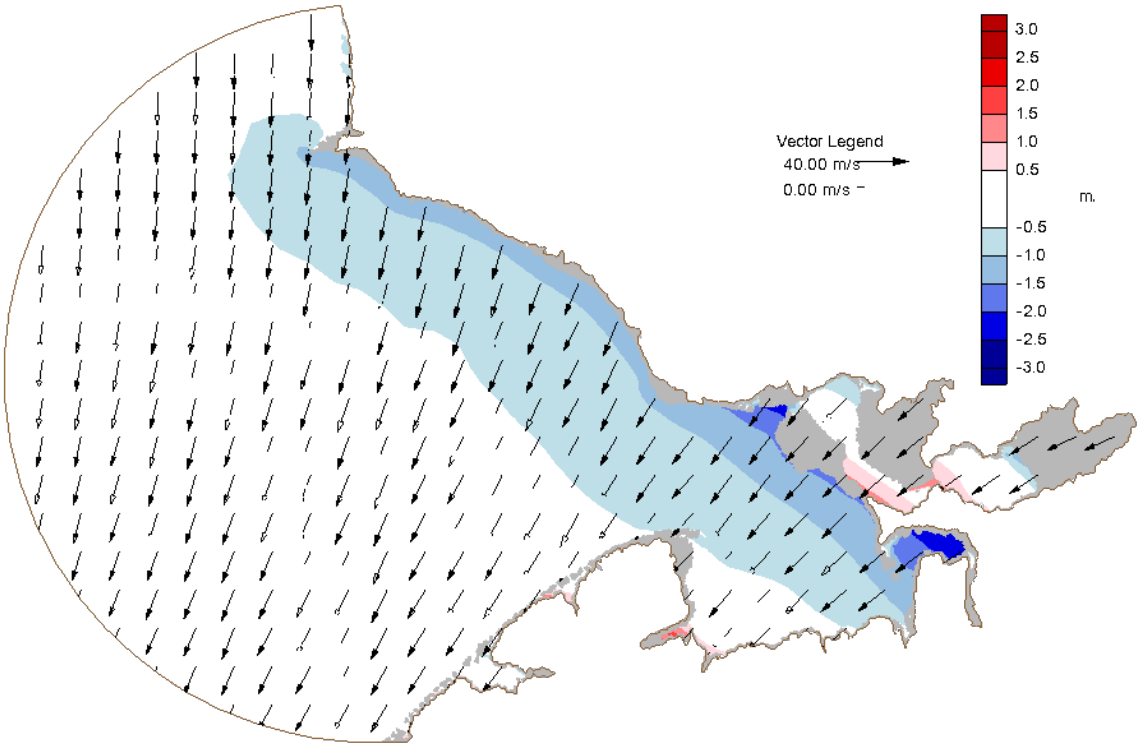

Figure 3.24. Winds and water elevation for track SEC SS at 102 hours. Color filled contours are water elevation in meters relative to mean sea level with areas in gray indicating dry land within the domain. Vectors are 10 m wind velocity displayed on a constant grid.

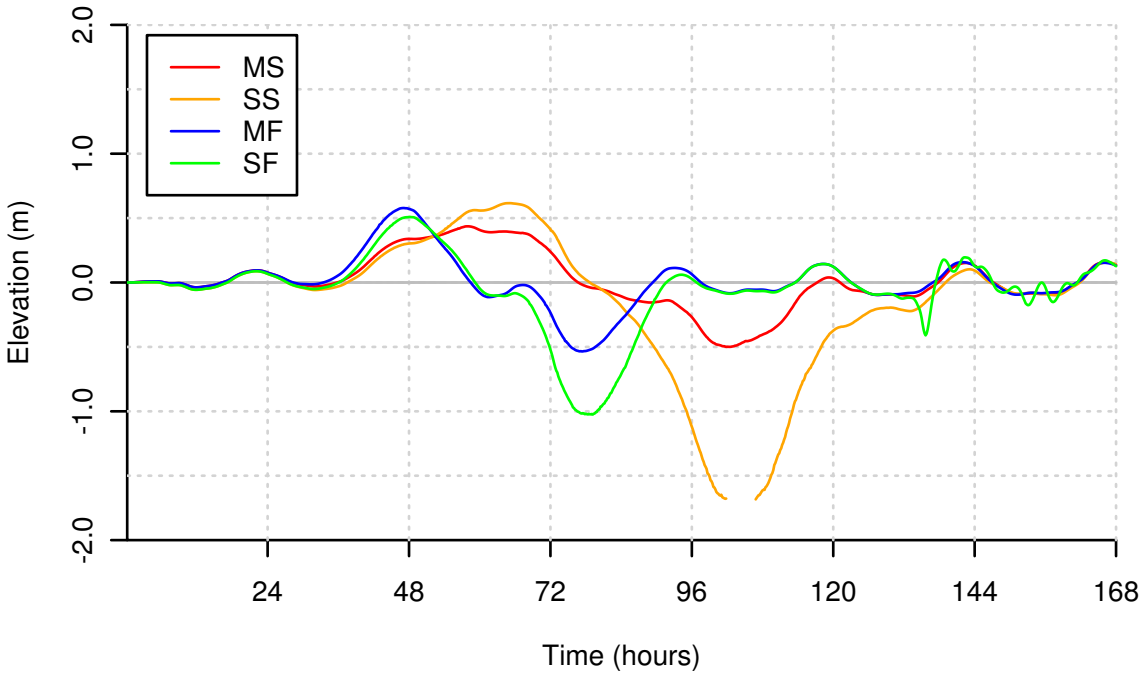

Figure 3.25. Time series of water elevation at Kotzebue for track SEC. Elevation in meters relative to mean sea level. Gap indicates model considered the recording station node to be dry.

The southern coast of the sound showed very little impact from the storm. Neither Deering nor Shishmaref showed water levels differing from tidal range by more than 0.2 m.

Currents around the entrance to Hotham Inlet show eddy circulation in addition to the larger scale flow. At hour 78, winds slacken following the positive surge (figure 3.26). Water is moving out of the inlet however, in spite of a component of the wind pushing in the opposite direction, due to imbalance of water levels (figure 3.27). At hour 102 winds pull water away from the inlet, but the entrance is too small to allow enough water through causing a negative surge west of the inlet (figures 3.28 and 3.29).

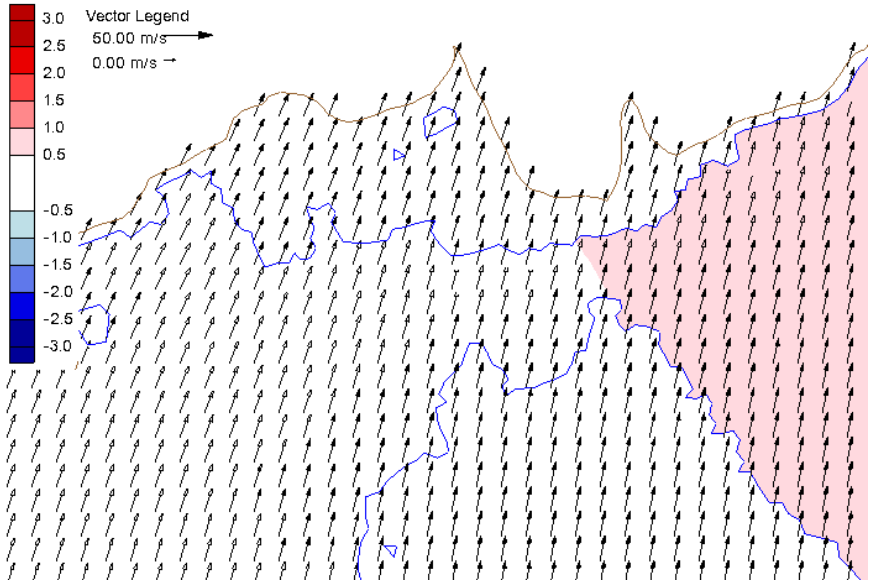

Figure 3.26. Winds and water elevation in Hotham Inlet entrance for SEC at hour 78. Color filled contours are water elevation in meters relative to mean sea level. Vectors are 10 m wind velocity displayed on a constant grid. Blue line indicates wet/dry boundary. Brown line indicates domain extent.

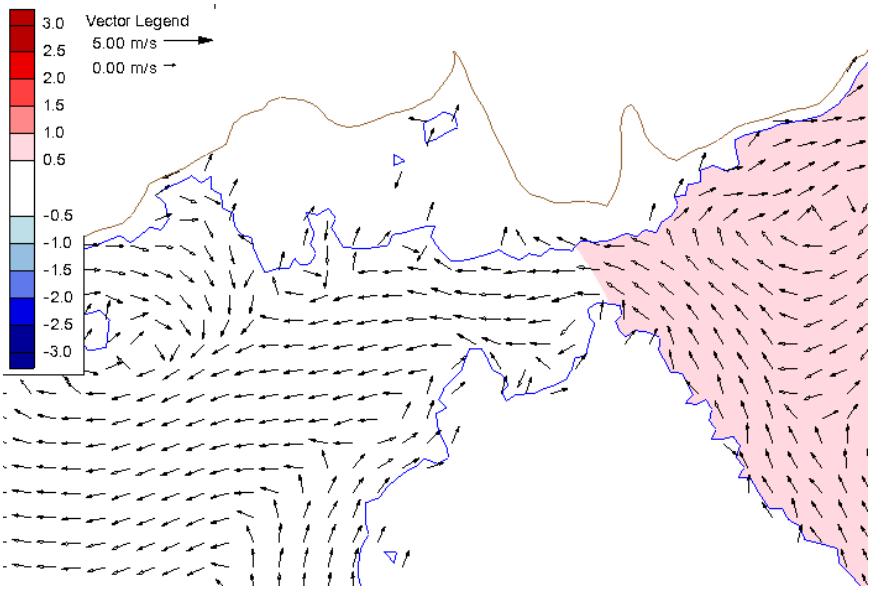

Figure 3.27. Water current and elevation in Hotham Inlet entrance for SEC at hour 78. Color filled contours are water elevation in meters relative to mean sea level. Vectors are depth-averaged current velocity displayed on a constant grid. Blue line indicates wet/dry boundary. Brown line indicates domain extent.

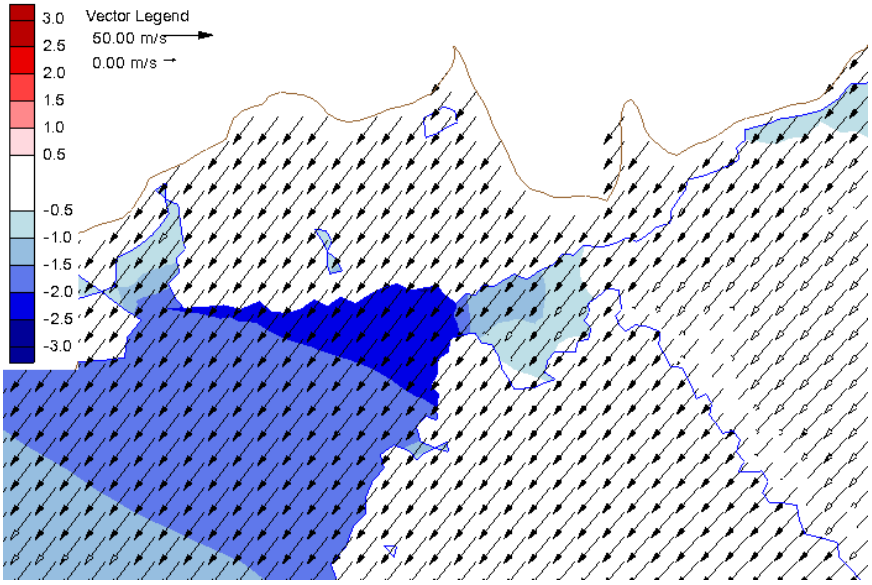

Figure 3.28. Winds and water elevation in Hotham Inlet entrance for SEC at hour 102. Color filled contours are water elevation in meters relative to mean sea level. Vectors are 10 m wind velocity displayed on a constant grid. Blue line indicates wet/dry boundary. Brown line indicates domain extent.

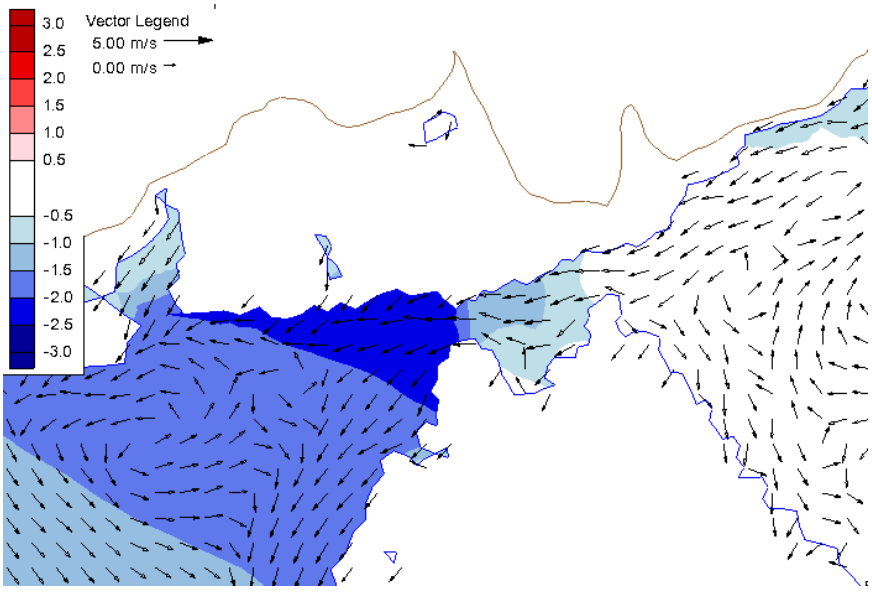

Figure 3.29. Water current and elevation in Hotham Inlet entrance for SEC at hour 102. Color filled contours are water elevation in meters relative to mean sea level. Vectors are depth-averaged current velocity displayed on a constant grid. Blue line indicates wet/dry boundary. Brown line indicates domain extent.

3.2 Comparisons with real world data

Six minute water level data were obtained from the National Oceanic and Atmospheric Administration (NOAA) National Ocean Service (NOS) water level recording station at the Red Dock Port facility. Using the residual data eleven positive surge events (verified tide gauge measurement minus predicted tide level) exceeding 1 m were identified. The weather pattern on these dates was analyzed by plotting sea level pressure daily composite charts from the NCEP/NCAR Reanalysis (Kalnay et al., 1996).

The storms that generated these events may be generally grouped as follows: nine moved northeast from the Bering Sea, one moved east along the arctic coast and one remained stationary in the central Bering Sea. Storm ground track speeds of the non-stationary storms varied from 400 km to 800 km per day, or between 15 km/h and 35 km/h.

From October 19 through 21, 2004, a low pressure system moved northeastward through the Bering Sea following a track in between BS1 and BS2 of this study. The storm center moved approximately 500 km from October 18 to 19, and then moved just 100 km per day in a clockwise arc around the end of the Siberian Peninsula. Water levels reached 1.5 m.

On December 26, 2004, a low followed a track similar to BS1 of this study. From December 25 to 26 the storm traveled 800 km from Kamchatka to the Chukchi Sea, although elongation of the low pressure feature acted to confound an accurate assessment of track speed. A high pressure ridge was set up southwest-northeast across Alaska at around 1035 hPa. The presence of this high pressure in proximity to the low increases the pressure gradient between the two and thus increasing wind speeds. Water levels reached 1.97 m,

the highest level ever recorded by the gauge.

On January 3 and 4, 2005 a storm transited through the western Bering and across the Siberian Peninsula and north up the date line. From January 2 to 3, the storm travelled 500 km before going 1000 km north from January 3 to 4. The maximum water level reached 1.4 m.

On August 7 and 8, 2005, a low pressure complex with centers in western Bering and Eastern Siberian seas and a 1025 hPa high in the Gulf of Alaska set up. The two lows moved northward 800 km per day, leaving a similar pattern both days. The resulting pressure gradient caused a surge reaching 1.4 m.

On September 23 and 24, 2005, a low set up near the end of the Siberian Peninsula, moving northwest around 400 km per day along a track similar to BS1. Ridges of high pressure were present in the Gulf of Alaska and northern Beaufort Sea. Water levels reached 1.5 m.

On February 19 and 20, 2006, a storm moved across the Siberian Peninsula to north of Barrow approximately 600 km per day. A 1040 hPa ridge had its axis northwest through British Columbia. The resulting water level reached 1.1 m.

On December 1 and 2, 2006, a low transited from near St. Lawrence Island north-northwestwards to the East Siberian Sea at approximately 600 km per day, while high pressure built over Alaska reaching 1035 hPa on December 2. Water levels reached 1.1 m. This event had no direct analogue in the storm track categories employed in this study.

On September 10, 2007, a stationary low was in the central Bering Sea while a ridge

was in place centered on 140W. Water level reached 1 m. This event also had no direct analog in the storm tracks considered.

On January 20 and 21, 2008, a low made its way north along the 180th meridian at 700 km per day while a 1030 hPa ridge was set up over Alaska and Western Canada. Water level reached 1.4 m.

On December 15, 2008, strong high pressure (1045 hPa+) centered in the Yukon expanded westward into Alaska, as a weak low at 72N moved eastward across the Arctic coast. The storm ground track speed averaged 500 km per day. This was similar to track AE1 of this study. Water level reached 0.9 m with a surge just over 1 m.

On September 1, 2009, a low transiting eastern Siberia in a northeastward reached the Chukchi Sea, moving at 400 km per day. Water level reached 1.1 m.

Storms showing a consistent track and track speed similar to idealized tracks considered in the model simulations showed a largely symmetric time series. The January 2008 storm was an example of this, with both the rise and fall of water taking around 30 hours (see figure 3.30). This compares favorably with the pattern seen in the model time series of Red Dog for storm SS on track BS2, which shows a similar symmetric pattern (figure 3.31).

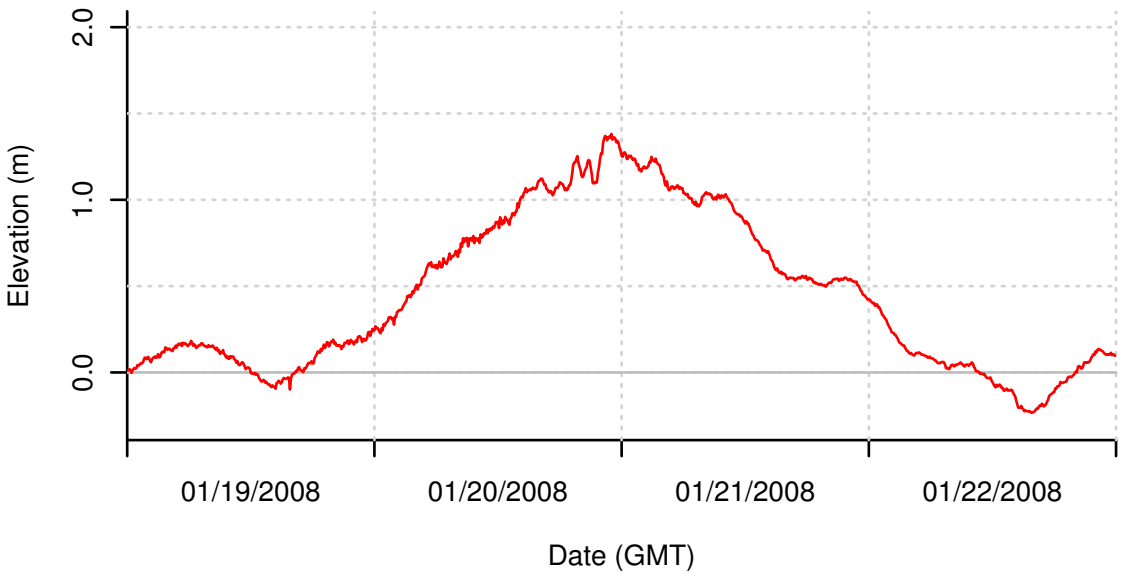

Figure 3.30. Observed water elevation at Red Dog Dock during January 2008 storm. Expressed in meters relative to mean sea level.

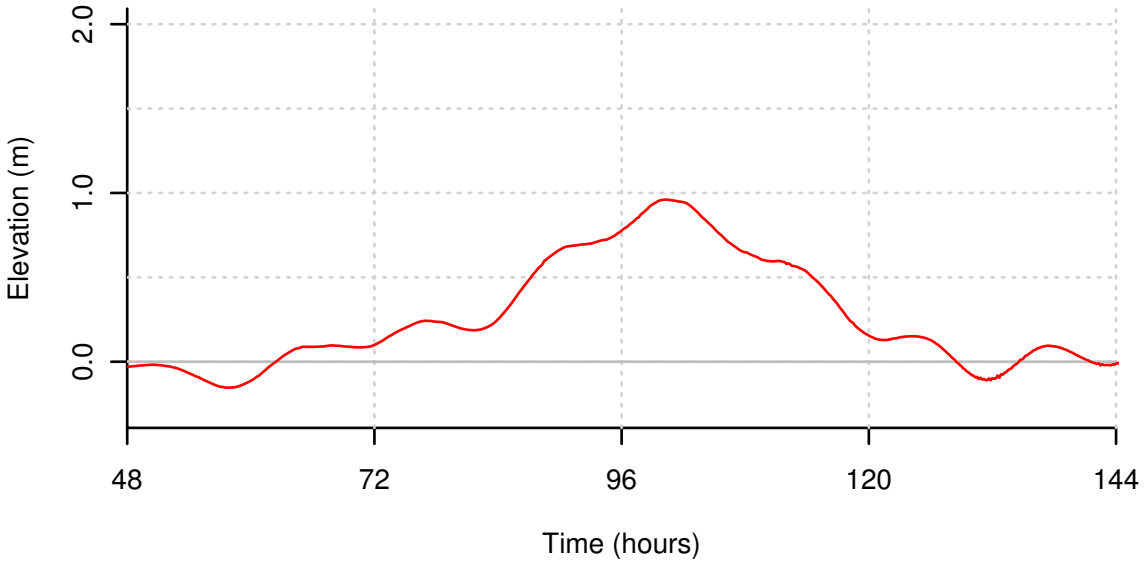

Figure 3.31. Time series of water elevation at Red Dog for track BS2. Elevation in meters relative to mean sea level.

The form of time series is dependent on the track and track speed however, which

remains constant in the idealized storms but can vary considerably in observed storms. The October 2004 storm, for example, first followed a track similar BS2 and at a speed similar to slower storms considered. After October 19, the storm slowed to 100 km per day while undergoing cyclolysis near the Bering Strait. The continued proximity of the storm to Kotzebue Sound kept water levels elevated for an extended period following the peak, creating a positive skew to the time series (figure 3.32).

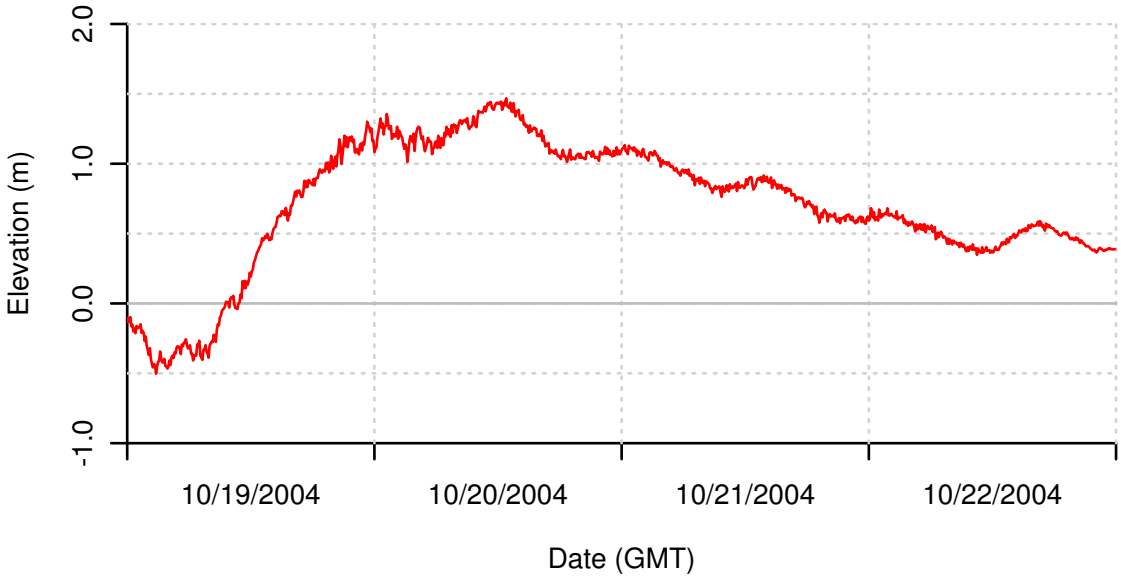

Figure 3.32. Observed water elevation at Red Dog Dock during October 2004 storm. Expressed in meters relative to mean sea level.

This review of observed events indicates two things: the tracks and storm propagation speeds used in this study were reasonable analogues to real tracks, and the magnitudes and forms of the modeled surge responses were realistic when compared to real events. This indicates that this modelling approach, even using idealized storm presentations, forms a useful tool for assessing possible surge responses.

Chapter 4

Conclusions

4.1 Discussion

This study has suggested the usefulness of applying this sort of surge model to learn about water set up, set down and associated induced current responses on the Alaskan coast. The approach allows detailed examination of the local effects caused by atmospheric synoptic drivers, providing an understanding of how surge affects particular areas.

In Hotham Inlet east of Baldwin Peninsula, at least some flooding was seen for all storm tracks. This is of note because the body of water has very little possible fetch. All but a small entrance to the inlet is blocked by the peninsula, leaving a maximum potential fetch of only 10 km. The timings of peak water elevations lag behind those on the other side of Baldwin Peninsula in Kotzebue Sound by 24 hours. This suggests that water is transported into the inlet only after enough has been driven into eastern Kotzebue Sound. This excess water then drains through the narrow entrance in to the inlet, resulting in the delayed timing of the peak.

The flooding of Hotham Inlet has a potentially large impact on the ecosystem there. Communication between the inlet and the sound is limited by the narrow passage and small tidal forcing. This allows the waters of the inlet to reach a brackish state, a result of fresh water input from the Kobuk and Selawik rivers diluting the saline water. The *inconnu* for example, a freshwater fish in the region, overwinters in Hotham Inlet, but it unable to survive in the marine waters of Kotzebue Sound (Hander et al., 2008). Thus flushing the

inlet with marine water would be detrimental to this fish.

The surge-driven current velocities through the narrow entrance were such that it could act to prevent the natural closing of the passage due to sedimentation from the Noatak River.

There is a noticeable difference in surge magnitude between storms of differing ground track speed for all tracks. Simply put, the slower a storm moves through the area, the more time winds have to apply forcing to the water running up the surge height. This effect is amplified by storms that continue to intensify while affecting the region.

4.2 Limitations

A few simplifications were made in the implementation of this study. Storms were treated as symmetrical, which is typically rare for an extra-tropical cyclone for reasons of topography, differential temperatures, and dynamics. Track speed is likewise not uniform over a storm lifetime as treated in this study, but instead varies with the stage of storm development and the strength of upper level atmospheric forcing.

The grid domain was limited in extent. The Bering Strait was not within the domain limiting the accounting for tunneling of winds and currents through the narrow straight. The open ocean boundary was placed as far from the center of Kotzebue Sound as possible, but this meant that the boundary was close to the Eurasian landmass, limiting the model's ability to contend with the actual forcing of fetch on the ocean past this boundary.

Despite these limitations, the model was still very useful in studying the effects of surge on Kotzebue Sound. The observational comparison suggests that the results are reasonable.

4.3 Future work

Running ADCIRC using more realistic atmospheric forcing could potentially yield better results by more explicitly accounting for the structure of the atmospheric forcing parameters.

Accounting for the influence of sea ice, specifically distance to the pack edge, could be useful as this northerly area on average has sea ice for a large portion of the year, including the late fall/early winter when there are still strong storms entering the area. Adding information about pack ice, perhaps as a surrogate land boundary in incorporating it in the model environment, could act to more realistically limit surge response when the pack ice is close to shore.

References

Amante, C. and B. W. Eakins, 2009: ETOPO1 1 Arc-Minute Global Relief Model: Procedures, Data Sources and Analysis. *NOAA Technical Memorandum*, **NESDIS NGDC-24**, 19.

Anthes, R. A., 1982: *Tropical cyclones: their evolution, structure and effects*. Amer Meteorological Society, Boston, MA. ISBN 0933876548.

Atkinson, D. E., 2005: Observed Storminess Patterns and Trends in the Circum-Arctic Coastal Regime. *Geo-Mar. Lett.*, **25**(2-3), 98–109. ISSN 0276-0460. doi: 10.1007/s00367-004-0191-0.

Blier, W., S. Keefe, W. A. Shaffer and S. C. Kim, 1997: Storm Surges in the Region of Western Alaska. *Mon. Wea. Rev.*, **125**(12), 3094–3108.

Cabanes, C., A. Cazenave and C. L. Provost, 2001: Sea Level Rise During Past 40 Years Determined from Satellite and in Situ Observations. *Science*, **294**(5543), 840–842. doi: 10.1126/science.1063556.

Colle, B. A., F. Buonaiuto, M. J. Bowman, R. E. Wilson, R. Flood, R. Hunter, A. Mintz and D. Hill, 2008: New York City's Vulnerability to Coastal Flooding. *Bull. Amer. Met. Soc.*, **89**(6), 829–841.

Fathauer, T., 1975: The great Bering Sea storms of 9-12 November 1974. *Weatherwise*, (28), 76–83.

Garratt, J., 1977: Review of Drag Coefficients over Oceans and Continents. *Mon. Wea. Rev.*, **105**(7), 915–929.

Hander, R. F., R. J. Brown and T. J. Underwood, 2008: Comparison of Inconnu Spawning Abundance Estimates in the Selawik River, 1995, 2004, and 2005, Selawik National Wildlife Refuge. Technical report, U.S. Fish and Wildlife Service, Fairbanks, Alaska.

Hume, J. D. and M. Schalk, 1967: Shoreline processes near Barrow, Alaska: A comparison of the normal and the catastrophic. *Arctic*, **20**(2), 86–103.

Hupp, J. W., J. A. Schmutz and C. R. Ely, 2008: The annual migration cycle of emperor geese in western Alaska. *Arctic*, **61**(1), 23–34.

Johnson, W. R. and Z. Kowalik, 1986: Modeling of Storm Surges in the Bering Sea and Norton Sound. *J. Geophys. Res.*, **91**(C4), 5119–5128. ISSN 0148-0227. doi: 10.1029/JC091iC04p05119.

Kalnay, E., M. Kanamitsu, R. Kistler, W. Collins, D. Deaven, L. Gandin, M. Iredell, S. Saha, G. White, J. Woollen et al., 1996: The NCEP/NCAR 40-year reanalysis project. *Bull. Amer. Met. Soc.*, **77**(3), 437–472.

Kowalik, Z., 1984: Storm Surges in the Beaufort and Chukchi Seas. *J. Geophys. Res.*, **89**(C6), 10,570–10,578.

Larsen, C., D. E. Atkinson, J. Walsh, J. Arnott and J. Lingaas, 2006: Dynamical Development of the Bering/Chukchi Sea Storm, October, 2004. In *AGU Fall Meeting Abstracts*, page 0827.

Lowe, J. and J. Gregory, 2005: The Effects of Climate Change on Storm Surges Around the United Kingdom. *Phil. Trans. R. Soc. A*, **363**(1831), 1313–1328. doi: 10.1098/rsta.2005.1570.

Lynch, A. H., E. N. Cassano, J. J. Cassano and L. R. Lestak, 2003: Case Studies of High Wind Events in Barrow, Alaska: Climatological Context and Development Processes. *Mon. Wea. Rev.*, **131**(4), 719–732.

Mason, O. K., W. J. Neal and O. H. Pilkey, 1997: *Living with the Coast of Alaska*. Duke University Press. ISBN 0822320193, 9780822320197.

Mendelsohn, R. and J. E. Neumann, 2004: *The Impact of Climate Change on the United States Economy*. Cambridge University Press. ISBN 0521607698.

Parkinson, C. L., D. J. Cavalieri, P. Gloersen, H. J. Zwally and J. C. Comiso, 1999: Arctic sea ice extents, areas, and trends, 1978-1996. *J. Geophys. Res.*, **104**(C9), 20,837–20,856. doi:10.1029/1999JC900082.

Parry, M., 2007: *Climate change 2007: impacts, adaptation and vulnerability : contribution of Working Group II to the fourth assessment report of the Intergovernmental Panel on Climate Change*. Cambridge University Press, Cambridge, U.K. ISBN 9780521880107.

Pickard, G. L. and S. Pond, 1983: *Introductory Dynamical Oceanography, Second Edition*. Butterworth-Heinemann, 2nd edition. ISBN 0750624965.

Reimnitz, E. and D. K. Maurer, 1979: Effects of storm surges on the Beaufort Sea coast, northern Alaska. *Arctic*, **32**(4), 329–344.

Rodionov, S., N. Bond and J. Overland, 2007: The Aleutian Low, storm tracks, and winter climate variability in the Bering Sea. *Deep Sea Research Part II: Topical Studies in Oceanography*, **54**(23-26), 2560–2577. ISSN 0967-0645. doi: 10.1016/j.dsr2.2007.08.002.

Schafer, P., 1966: Computation of a Storm Surge at Barrow, Alaska. *Meteorol. Atmos. Phys.*, **15**(3), 372–393. doi:10.1007/BF02247222.

US Army Corps of Engineers Alaska District, 2006: Alaska Village Erosion Technical Assistance Program. Technical report.

US Census Bureau, 2009: *Statistical Abstract of the United States: 2010*. Washington, DC, 129th edition.

Westerink, J. J., R. A. Luettich, J. C. Feyen, J. H. Atkinson, C. Dawson, H. J. Roberts, M. D. Powell, J. P. Dunion, E. J. Kubatko and H. Pourtaheri, 2008: A Basin- to Channel-Scale Unstructured Grid Hurricane Storm Surge Model Applied to Southern Louisiana. *Mon. Wea. Rev.*, **136**(3), 833–864.

Williams, J., J. J. Higginson and J. D. Rohrbough, 1973: *Sea and Air: The Marine Environment*. Naval Institute Press, 2nd edition. ISBN 0870215965.

Wise, J. L., A. L. Comiskey and R. Becker, 1981: Storm surge climatology and forecasting in Alaska. *Arctic Environmental Information and Data Center, University of Alaska, Anchorage, Alaska*.

Appendix A

stormgen.ncl

stormgen.ncl is an NCL program developed to generate wind and pressure input on a regular grid using idealized storm scenarios for use in circulation and surge models.

```
load "$NCARG_ROOT/lib/ncarg/nclscripts/csm/gsn_code.ncl"
load "$NCARG_ROOT/lib/ncarg/nclscripts/csm/gsn_csm.ncl"
load "$NCARG_ROOT/lib/ncarg/nclscripts/csm/contributed.ncl"

begin

;***********************************************
; User input storm parameters
;***********************************************

stormStartX = -170  ; start latitude
stormStartY = 72    ; start longitude
stormHead   = 270   ; storm heading
stormVel    = 20    ; storm velocity (km/day)
centP_start = 000   ; starting pressure (gzpm)
centP_trend = 40    ; pressure trend (gzpm/day)

backgnd_P   = 150   ; background pressure field
Pramp2_rad  = 3000  ; radius of the main system in km

;*************************************************************

; define spline curve
xi = (/0, 5, 30, 80, 100/)
yidef = (/0., 5., 60., 98., 100./)

; scale to storm radius
xi = xi*(3000/100)
xo = fspan(0,3000,500)

; set up output grid
boxStartX   = -180  ; output box LL corner X (lon)
boxStartY   = 75    ; output box UL corner Y (lat)
boxStepX    = 0.25  ; grid del x in degrees
boxStepY    = -0.25 ; grid del y in degrees
boxNX       = 101   ; number of grid points X
```

```
boxNY       = 61    ; number of grid points Y

; timestep information
time_step   = 3          ; hours between each wind ob
totalSteps  = 57    ; 3-hly, 7 days
startstep   = 10    ; timestep where storm begins moving

; constants
d2r         = 0.017453
diameter    = 12741
pi          = 3.14159

; distance travelled in one time step, in radians
d_rads = ((stormVel*time_step)/(pi*diameter))*2*pi
; standardize P trend per time step interval
centP_ts = centP_trend/(24/time_step)
; array for storm center coords
strmcent = new(totalSteps,"string")

;*** set up target grids
targ = new((/totalSteps,boxNY,boxNX/),"float")
targ_out = targ
P = targ ; set up dummy pressure grid

time = ispan(1,totalSteps,1)          ; build a time variable
lat_vect = fspan(boxStartY,boxStartY+(boxNY-1)*boxStepY,boxNY)
lon_vect = fspan(boxStartX,boxStartX+(boxNX-1)*boxStepX,boxNX)
lat_vect@units = "degrees_north"
lon_vect@units = "degrees_east"

P!0    = "time"
P!1    = "lat"
P!2    = "lon"

P&time = time
P&lat  = lat_vect
P&lon  = lon_vect

do timeStep = 1,totalSteps
     ; establish the parameters that change with each TS
     if (timeStep.lt.startstep) then
          Storm_centP = centP_start ; in Pascals
```

```
     ; storm start position, long
     Storm_currX = int2flt(stormStartX)
     ; storm start position, lat
     Storm_currY = int2flt(stormStartY)

     oldX = Storm_currX
     oldY = Storm_currY
end if

if (timeStep.ge.startstep) then
     oldX = Storm_currX
     oldY = Storm_currY
     ; in Pascals/time step
     Storm_centP = Storm_centP + centP_ts
     Storm_currY = asin(sin(Storm_currY*d2r)*cos(d_rads)+ \
          cos(Storm_currY*d2r)*sin(d_rads)* \
          cos(stormHead*d2r))/d2r
     if (cos(Storm_currY*d2r).eq.0) then
          Storm_currX = Storm_currX
     else
          Storm_currX = (mod(Storm_currX*d2r - \
               asin(sin(-1*stormHead*d2r)*sin(d_rads)/ \
               cos(Storm_currY*d2r))+pi,2*pi)-pi)/d2r
     end if
end if

diffX = decimalPlaces(Storm_currX-oldX,2,True)
diffY = decimalPlaces(Storm_currY-oldY,2,True)

strmcent(timeStep-1) = decimalPlaces(Storm_currY,2,True) \
     + ", " + decimalPlaces(Storm_currX,2,True) + ", hr " \
     + (timeStep-1)*time_step + " p " + Storm_centP

; Build the overall pressure gradient <not used>
yi = yidef*((int2flt(backgnd_P)-int2flt(Storm_centP))/100)
yo = ftcurv(xi, yi, xo)

do lat_step = 1,boxNY
     do lon_step = 1,boxNX
          lat = boxStartY + boxStepY*(lat_step-1)
          lon = boxStartX + boxStepX*(lon_step-1)
```

```
                dist = diameter*asin(sqrt(1-cos(Storm_currY*d2r)*\
                     cos(lat*d2r)*cos(lon*d2r-Storm_currX*d2r)\
                     -sin(Storm_currY*d2r)*sin(lat*d2r)))

                if (timeStep.lt.startstep) then
                     if (dist.gt.Pramp2_rad) then
                          P(timeStep-1,lat_step-1,lon_step-1) = \
                          backgnd_P + random_normal(0,.02,(/1/))
                     else
                          pchdist = yo(closest_val(dist,xo))
                          P(timeStep-1,lat_step-1,lon_step-1) = \
                          Storm_centP + pchdist \
                          + random_normal(0,.02,(/1/))
                     end if
                else
                     if (dist.gt.Pramp2_rad) then
                          P(timeStep-1,lat_step-1,lon_step-1) = \
                          backgnd_P + random_normal(0,.02,(/1/))
                     else
                          pchdist = yo(closest_val(dist,xo))
                          P(timeStep-1,lat_step-1,lon_step-1) = \
                          (Storm_centP + centP_ts) +  pchdist \
                          + random_normal(0,.02,(/1/))
                     end if
                end if

                targ(timeStep-1,lat_step-1,lon_step-1) = dist
           end do; lon
      end do ; lat

; Determine the windfield from the P field
uv = z2geouv (P,lat_vect,lon_vect,0)

u           = uv(0,:,:,:)     ; u(nlat,mlon)
u@long_name = "geostrophic zonal wind component"
u@units     = "m/s"

u!0    = "time"
u!1    = "lat"
u!2    = "lon"

u&time = time
```

```
u&lat  = lat_vect
u&lon  = lon_vect

v           = uv(1,:,:,:)     ; u(nlat,mlon)
v@long_name = "geostrophic meridional wind component"
v@units     = "m/s"

v!0    = "time"
v!1    = "lat"
v!2    = "lon"

v&time = time
v&lat  = lat_vect
v&lon  = lon_vect

targ_out = targ(:,::-1,:)
P_out = P(:,::-1,:)
realP_out = (1000-((backgnd_P-P_out)/8.2))*100
v_out = v(:,::-1,:)
u_out = u(:,::-1,:)

; total number of grid points + space after each longitude vector
npts  = dimsizes(lat_vect)*dimsizes(lon_vect)*totalSteps \
     + (totalSteps*dimsizes(lat_vect))

fName = "fort.22"
data  = new( npts, "string")

npt = -1
do ts=0,totalSteps-1
     do nl=0,dimsizes(lat_vect)-1
          do ml=0,dimsizes(lon_vect)-1

               npt  = npt + 1

               data(npt) = sprintf("%5.2f ",u_out(ts,nl,ml))
               data(npt) = data(npt) \
                    + sprintf("%5.2f ",v_out(ts,nl,ml))
               data(npt) = data(npt) \
                    + sprintf("%8.0f",realP_out(ts,nl,ml))

          end do
```

```
          npt  = npt + 1
          data(npt) = "  "
     end do
end do

asciiwrite (fName , data)

fName = "stormcenter.csv"
asciiwrite (fName, strmcent)

end
```

Appendix B

fort.15

The fort.15 file is input data for the ADCIRC model that contains most of the parameters required to run the model.

```
 ! 32 CHARACTER ALPHANUMERIC RUN DESCRIPTION
 ! 24 CHARACTER ALPHANUMERIC RUN IDENTIFICATION
1 ! NFOVER - NONFATAL ERROR OVERRIDE OPTION
0 ! NABOUT - ABREVIATED OUTPUT OPTION PARAMETER
1 ! NSCREEN - OUTPUT TO UNIT 6 PARAMETER
0 ! IHOT - HOT START OPTION PARAMETER
2 ! ICS - COORDINATE SYSTEM OPTION PARAMETER
0 ! IM - MODEL RUN TYPE: 0,10,20,30=2DDI, 1,11,21,31=3D(VS), 2=3D(DSS)
1 ! NOLIBF - NONLINEAR BOTTOM FRICTION OPTION
2 ! NOLIFA - OPTION TO INCLUDE FINITE AMPLITUDE TERMS
1 ! NOLICA - OPTION TO INCLUDE CONVECTIVE ACCELERATION TERMS
1 ! NOLICAT - OPTION TO CONSIDER TIME DERIVATIVE OF CONV ACC TERMS
0 ! NWP - Number of nodal attributes.
0 ! NCOR - VARIABLE CORIOLIS IN SPACE OPTION PARAMETER
1 ! NTIP - TIDAL POTENTIAL OPTION PARAMETER
6 ! NWS - WIND STRESS AND BAROMETRIC PRESSURE OPTION PARAMETER
1 ! NRAMP - RAMP FUNCTION OPTION
9.80665 ! G - ACCELERATION DUE TO GRAVITY - DETERMINES UNITS
0.01000 ! TAU0 - WEIGHTING FACTOR IN GWCE
5.00000 ! DT - TIME STEP (IN SECONDS)
0.00000 ! STATIM - STARTING SIMULATION TIME IN DAYS
0.00000 ! REFTIME - REFERENCE TIME (IN DAYS)
61 101 75.000000 -180.000000 0.250000 0.250000 10800 ! MET SPECS
7.00000 ! RNDAY - TOTAL LENGTH OF SIMULATION (IN DAYS)
0.20000 ! DRAMP - DURATION OF RAMP FUNCTION (IN DAYS)
0.350000 0.300000 0.350000 ! TIME WEIGHTING FACTORS FOR GWCE
0.050000 12 12 0.050000 ! H0, NODEDRYMIN, NODEWETMIN, VELMIN
-166.344750 67.222155 ! SLAM0, SFEA0 - CPP COORDINATE CENTER
0.002500 ! FFACTOR - 2DDI BOTTOM FRICTION COEFFICIENT
2.000000 ! EVM - SPATIALLY CONSTANT HORIZONTAL EDDY VISCOSITY
0.000100 ! CORI - CONSTANT CORIOLIS COEFFICIENT
5 ! NTIF - NUMBER OF TIDAL POTENTIAL CONSTITUENTS
K1 ! TIPOTAG - NAME OF TIDAL POTENTIAL CONSTITUENT
0.14156500 0.000072921158358 0.736 1.072 166.445 ! CONST PROPERTIES
M2 ! TIPOTAG - NAME OF TIDAL POTENTIAL CONSTITUENT
```

```
0.24233400 0.000140518902509 0.693 0.980 170.303 ! CONST PROPERTIES
N2 ! TIPOTAG - NAME OF TIDAL POTENTIAL CONSTITUENT
0.04639800 0.000137879699487 0.693 0.980 111.355 ! CONST PROPERTIES
O1 ! TIPOTAG - NAME OF TIDAL POTENTIAL CONSTITUENT
0.10051400 0.000067597744151 0.695 1.116 1.006 ! CONST PROPERTIES
S2 ! TIPOTAG - NAME OF TIDAL POTENTIAL CONSTITUENT
0.11284100 0.000145444104333 0.693 1.000 0.000 ! CONST PROPERTIES
5 ! NBFR - NUMBER OF PERIODIC FORCING FREQUENCIES
K1 ! BOUNTAG - FORCING CONSTITUENT NAME
0.000072921158358 1.072 166.445
M2 ! BOUNTAG - FORCING CONSTITUENT NAME
0.000140518902509 0.980 170.303
N2 ! BOUNTAG - FORCING CONSTITUENT NAME
0.000137879699487 0.980 111.355
O1 ! BOUNTAG - FORCING CONSTITUENT NAME
0.000067597744151 1.116 1.006
S2 ! BOUNTAG - FORCING CONSTITUENT NAME
0.000145444104333 1.000 0.000
K1 ! EALPHA - FORCING CONSTITUENT NAME AGAIN
0.000000 0.000 ! EMO, EFA
0.000000 0.000 ! EMO, EFA
0.000000 0.000 ! EMO, EFA
0.000000 0.000 ! EMO, EFA
0.000000 0.000 ! EMO, EFA
0.000000 0.000 ! EMO, EFA
0.000000 0.000 ! EMO, EFA
0.000000 0.000 ! EMO, EFA
0.000000 0.000 ! EMO, EFA
0.000000 0.000 ! EMO, EFA
0.046700 71.700 ! EMO, EFA
0.046700 71.700 ! EMO, EFA
0.046700 71.700 ! EMO, EFA
0.046700 71.700 ! EMO, EFA
0.046700 71.700 ! EMO, EFA
0.046700 71.700 ! EMO, EFA
0.046700 71.700 ! EMO, EFA
0.046700 71.700 ! EMO, EFA
0.046700 71.700 ! EMO, EFA
0.046700 71.700 ! EMO, EFA
0.046700 71.700 ! EMO, EFA
0.046700 71.700 ! EMO, EFA
0.046615 71.769 ! EMO, EFA
```

```
0.045424 71.601 ! EMO, EFA
0.042879 70.366 ! EMO, EFA
0.039476 69.202 ! EMO, EFA
0.031377 66.470 ! EMO, EFA
0.022627 62.680 ! EMO, EFA
0.015438 58.706 ! EMO, EFA
0.010357 57.942 ! EMO, EFA
0.006482 61.707 ! EMO, EFA
0.003416 60.627 ! EMO, EFA
0.000816 37.310 ! EMO, EFA
0.001627 259.103 ! EMO, EFA
0.003412 250.979 ! EMO, EFA
0.005705 251.869 ! EMO, EFA
0.007777 250.752 ! EMO, EFA
0.009203 249.775 ! EMO, EFA
0.008466 248.921 ! EMO, EFA
0.007657 248.589 ! EMO, EFA
0.006783 249.535 ! EMO, EFA
0.005905 252.601 ! EMO, EFA
0.005060 257.217 ! EMO, EFA
0.004344 263.842 ! EMO, EFA
0.003818 273.205 ! EMO, EFA
0.003477 284.555 ! EMO, EFA
0.003376 296.949 ! EMO, EFA
0.003521 309.266 ! EMO, EFA
0.003831 318.757 ! EMO, EFA
0.004210 324.633 ! EMO, EFA
0.004594 328.309 ! EMO, EFA
0.004874 330.274 ! EMO, EFA
0.005018 332.931 ! EMO, EFA
0.005128 335.015 ! EMO, EFA
0.005217 336.576 ! EMO, EFA
0.005285 337.690 ! EMO, EFA
M2 ! EALPHA - FORCING CONSTITUENT NAME AGAIN
0.000000 0.000 ! EMO, EFA
0.000000 0.000 ! EMO, EFA
0.000000 0.000 ! EMO, EFA
0.000000 0.000 ! EMO, EFA
0.000000 0.000 ! EMO, EFA
0.000000 0.000 ! EMO, EFA
0.000000 0.000 ! EMO, EFA
0.000000 0.000 ! EMO, EFA
```

```
0.000000 0.000 ! EMO, EFA
0.000000 0.000 ! EMO, EFA
0.058600 80.600 ! EMO, EFA
0.058600 80.600 ! EMO, EFA
0.058600 80.600 ! EMO, EFA
0.058600 80.600 ! EMO, EFA
0.058600 80.600 ! EMO, EFA
0.058600 80.600 ! EMO, EFA
0.058600 80.600 ! EMO, EFA
0.058600 80.600 ! EMO, EFA
0.058600 80.600 ! EMO, EFA
0.058600 80.600 ! EMO, EFA
0.058600 80.600 ! EMO, EFA
0.058600 80.600 ! EMO, EFA
0.058747 80.594 ! EMO, EFA
0.060284 82.646 ! EMO, EFA
0.063557 87.962 ! EMO, EFA
0.068054 92.302 ! EMO, EFA
0.080969 92.872 ! EMO, EFA
0.093904 89.593 ! EMO, EFA
0.103413 82.815 ! EMO, EFA
0.108998 73.404 ! EMO, EFA
0.112669 61.589 ! EMO, EFA
0.110815 52.327 ! EMO, EFA
0.103159 45.027 ! EMO, EFA
0.088674 37.718 ! EMO, EFA
0.066807 30.609 ! EMO, EFA
0.036346 28.322 ! EMO, EFA
0.006854 46.737 ! EMO, EFA
0.017186 191.022 ! EMO, EFA
0.012111 189.984 ! EMO, EFA
0.007089 190.276 ! EMO, EFA
0.003298 201.908 ! EMO, EFA
0.002576 246.985 ! EMO, EFA
0.003164 276.098 ! EMO, EFA
0.003451 284.029 ! EMO, EFA
0.004207 269.736 ! EMO, EFA
0.004621 252.806 ! EMO, EFA
0.004952 230.337 ! EMO, EFA
0.005942 201.684 ! EMO, EFA
0.008256 179.116 ! EMO, EFA
0.010977 167.510 ! EMO, EFA
```

```
0.013663 161.311 ! EMO, EFA
0.015463 157.840 ! EMO, EFA
0.018085 160.288 ! EMO, EFA
0.020258 162.158 ! EMO, EFA
0.021959 163.359 ! EMO, EFA
0.023215 164.130 ! EMO, EFA
N2 ! EALPHA - FORCING CONSTITUENT NAME AGAIN
0.000000 0.000 ! EMO, EFA
0.000000 0.000 ! EMO, EFA
0.000000 0.000 ! EMO, EFA
0.000000 0.000 ! EMO, EFA
0.000000 0.000 ! EMO, EFA
0.000000 0.000 ! EMO, EFA
0.000000 0.000 ! EMO, EFA
0.000000 0.000 ! EMO, EFA
0.000000 0.000 ! EMO, EFA
0.000000 0.000 ! EMO, EFA
0.050300 119.200 ! EMO, EFA
0.050300 119.200 ! EMO, EFA
0.050300 119.200 ! EMO, EFA
0.050300 119.200 ! EMO, EFA
0.050300 119.200 ! EMO, EFA
0.050300 119.200 ! EMO, EFA
0.050300 119.200 ! EMO, EFA
0.050300 119.200 ! EMO, EFA
0.050300 119.200 ! EMO, EFA
0.050300 119.200 ! EMO, EFA
0.050300 119.200 ! EMO, EFA
0.050300 119.200 ! EMO, EFA
0.050254 119.235 ! EMO, EFA
0.049738 118.997 ! EMO, EFA
0.048731 117.907 ! EMO, EFA
0.047337 116.487 ! EMO, EFA
0.046557 114.293 ! EMO, EFA
0.045501 110.611 ! EMO, EFA
0.044097 105.503 ! EMO, EFA
0.042099 98.773 ! EMO, EFA
0.039389 90.083 ! EMO, EFA
0.035725 82.295 ! EMO, EFA
0.030937 76.154 ! EMO, EFA
0.024367 71.347 ! EMO, EFA
0.016507 70.211 ! EMO, EFA
```

```
0.010022 74.732 ! EMO, EFA
0.004822 102.072 ! EMO, EFA
0.004092 165.883 ! EMO, EFA
0.003007 161.058 ! EMO, EFA
0.001970 153.627 ! EMO, EFA
0.001136 149.533 ! EMO, EFA
0.000641 180.501 ! EMO, EFA
0.000679 222.984 ! EMO, EFA
0.000922 233.785 ! EMO, EFA
0.001391 230.245 ! EMO, EFA
0.001799 222.969 ! EMO, EFA
0.002121 213.117 ! EMO, EFA
0.002546 200.958 ! EMO, EFA
0.002974 189.008 ! EMO, EFA
0.003419 180.223 ! EMO, EFA
0.003877 174.206 ! EMO, EFA
0.004188 170.606 ! EMO, EFA
0.004723 170.488 ! EMO, EFA
0.005167 170.642 ! EMO, EFA
0.005511 170.748 ! EMO, EFA
0.005765 170.819 ! EMO, EFA
O1 ! EALPHA - FORCING CONSTITUENT NAME AGAIN
0.000000 0.000 ! EMO, EFA
0.000000 0.000 ! EMO, EFA
0.000000 0.000 ! EMO, EFA
0.000000 0.000 ! EMO, EFA
0.000000 0.000 ! EMO, EFA
0.000000 0.000 ! EMO, EFA
0.000000 0.000 ! EMO, EFA
0.000000 0.000 ! EMO, EFA
0.000000 0.000 ! EMO, EFA
0.000000 0.000 ! EMO, EFA
0.009600 100.900 ! EMO, EFA
0.009600 100.900 ! EMO, EFA
0.009600 100.900 ! EMO, EFA
0.009600 100.900 ! EMO, EFA
0.009600 100.900 ! EMO, EFA
0.009600 100.900 ! EMO, EFA
0.009600 100.900 ! EMO, EFA
0.009600 100.900 ! EMO, EFA
0.009600 100.900 ! EMO, EFA
0.009600 100.900 ! EMO, EFA
```

```
0.009600 100.900 ! EMO, EFA
0.009600 100.900 ! EMO, EFA
0.009581 101.160 ! EMO, EFA
0.009181 104.900 ! EMO, EFA
0.008366 114.208 ! EMO, EFA
0.007751 129.128 ! EMO, EFA
0.007424 171.029 ! EMO, EFA
0.011033 198.348 ! EMO, EFA
0.014979 204.714 ! EMO, EFA
0.017885 202.641 ! EMO, EFA
0.019743 198.633 ! EMO, EFA
0.019935 197.451 ! EMO, EFA
0.018684 198.579 ! EMO, EFA
0.016019 202.108 ! EMO, EFA
0.012637 209.744 ! EMO, EFA
0.010556 222.479 ! EMO, EFA
0.009327 241.748 ! EMO, EFA
0.009192 259.985 ! EMO, EFA
0.008615 259.884 ! EMO, EFA
0.007981 260.500 ! EMO, EFA
0.007277 262.126 ! EMO, EFA
0.006574 264.943 ! EMO, EFA
0.005914 269.214 ! EMO, EFA
0.005356 275.102 ! EMO, EFA
0.004941 281.997 ! EMO, EFA
0.004670 290.395 ! EMO, EFA
0.004673 299.773 ! EMO, EFA
0.004855 310.078 ! EMO, EFA
0.005357 318.713 ! EMO, EFA
0.005967 324.243 ! EMO, EFA
0.006565 327.784 ! EMO, EFA
0.007009 329.675 ! EMO, EFA
0.007175 332.002 ! EMO, EFA
0.007289 333.838 ! EMO, EFA
0.007383 335.228 ! EMO, EFA
0.007455 336.228 ! EMO, EFA
S2 ! EALPHA - FORCING CONSTITUENT NAME AGAIN
0.000000 0.000 ! EMO, EFA
0.000000 0.000 ! EMO, EFA
0.000000 0.000 ! EMO, EFA
0.000000 0.000 ! EMO, EFA
0.000000 0.000 ! EMO, EFA
```

```
0.000000 0.000 ! EMO, EFA
0.000000 0.000 ! EMO, EFA
0.000000 0.000 ! EMO, EFA
0.000000 0.000 ! EMO, EFA
0.000000 0.000 ! EMO, EFA
0.083000 112.300 ! EMO, EFA
0.083000 112.300 ! EMO, EFA
0.083000 112.300 ! EMO, EFA
0.083000 112.300 ! EMO, EFA
0.083000 112.300 ! EMO, EFA
0.083000 112.300 ! EMO, EFA
0.083000 112.300 ! EMO, EFA
0.083000 112.300 ! EMO, EFA
0.083000 112.300 ! EMO, EFA
0.083000 112.300 ! EMO, EFA
0.083000 112.300 ! EMO, EFA
0.083000 112.300 ! EMO, EFA
0.083048 112.358 ! EMO, EFA
0.082438 113.663 ! EMO, EFA
0.080421 116.796 ! EMO, EFA
0.078622 120.080 ! EMO, EFA
0.083049 122.748 ! EMO, EFA
0.088523 122.331 ! EMO, EFA
0.093201 118.131 ! EMO, EFA
0.096155 110.850 ! EMO, EFA
0.097864 100.915 ! EMO, EFA
0.094438 92.172 ! EMO, EFA
0.085886 84.373 ! EMO, EFA
0.071721 75.526 ! EMO, EFA
0.052554 65.486 ! EMO, EFA
0.031852 58.832 ! EMO, EFA
0.011897 47.171 ! EMO, EFA
0.005011 274.426 ! EMO, EFA
0.002525 281.895 ! EMO, EFA
0.000754 352.282 ! EMO, EFA
0.001873 52.310 ! EMO, EFA
0.002606 47.116 ! EMO, EFA
0.002844 46.142 ! EMO, EFA
0.002540 48.577 ! EMO, EFA
0.001610 37.506 ! EMO, EFA
0.000396 16.795 ! EMO, EFA
0.001252 211.035 ! EMO, EFA
```

```
0.003308 199.729 ! EMO, EFA
0.005692 192.992 ! EMO, EFA
0.007874 189.163 ! EMO, EFA
0.009817 186.865 ! EMO, EFA
0.011117 185.353 ! EMO, EFA
0.012797 188.439 ! EMO, EFA
0.014187 190.683 ! EMO, EFA
0.015279 192.147 ! EMO, EFA
0.016087 193.096 ! EMO, EFA
90 ! ANGINN - MINIMUM ANGLE FOR TANGENTIAL FLOW
-1 0.000000 7.000000 120 ! NOUTE, TOUTSE, TOUTFE, NSPOOLE
12 ! NSTAE, FOLLOWED BY LOCATIONS
-162.622057 66.907175
-162.050655 66.577744
-161.985768 66.629655
-162.369677 66.973537
-164.560000 67.720000
-164.088000 67.568000
-162.600000 66.897000
-164.540000 67.727000
-162.698000 66.087000
-166.118000 66.265000
-166.736000 68.320000
-166.736000 68.349300
-1 0.000000 7.000000 120 ! NOUTV, TOUTSV, TOUTFV, NSPOOLV
12 ! NSTAV, FOLLOWED BY LOCATIONS
-162.622057 66.907175
-162.050655 66.577744
-161.985768 66.629655
-162.369677 66.973537
-164.560000 67.720000
-164.088000 67.568000
-162.600000 66.897000
-164.540000 67.727000
-162.698000 66.087000
-166.118000 66.265000
-166.736000 68.320000
-166.736000 68.349300
-1 0.000000 7.000000 120 ! NOUTM, TOUTSM, TOUTFM, NSPOOLM
12 ! NSTAM, FOLLOWED BY LOCATIONS
-162.622057 66.907175
-162.050655 66.577744
```

```
-161.985768 66.629655
-162.369677 66.973537
-164.560000 67.720000
-164.088000 67.568000
-162.600000 66.897000
-164.540000 67.727000
-162.698000 66.087000
-166.118000 66.265000
-166.736000 68.320000
-166.736000 68.349300
-1 0.000000 7.000000 360 ! NOUTGE, TOUTSGE, TOUTFGE, NSPOOLGE
-1 0.000000 7.000000 360 ! NOUTGV, TOUTSGV, TOUTFGV, NSPOOLGV
-1 0.000000 7.000000 360 ! NOUTGM,TOUTSGM,TOUTFGM,NSPOOLGM
0 ! NHARF - NUMBER OF FREQENCIES IN HARMONIC ANALYSIS
0.000000 0.000000 0 0.000000 ! THAS,THAF,NHAINC,FMV
0 0 0 0 ! NHASE,NHASV,NHAGE,NHAGV
0 0 ! NHSTAR,NHSINC - HOT START FILE GENERATION PARAMETERS
1 0 1e-005 50 ! ITITER, ISLDIA, CONVCR, ITMAX
1 ! NUMBER OF PROCESSORS
```